FEDERAL UNIVERSITY OF ESPÍRITO SANTO - UFES
ELECTRICAL ENGINEERING POSTGRADUATE PROGRAM

Performance Evaluation of the LoRa Wide Area Network Technology

Menno Jan Faber

Supervisor: Dr. Sc. Jair Adriano Lima Silva

Co-Supervisor: PhD. Marcelo Eduardo Vieira Segatto

Vitória-ES
2020

Menno Jan Faber

Performance Evaluation of the LoRa Wide Area Network Technology

Dissertation submitted to the Electrical Engineering Postgraduate Program of the Technological Center of the Federal University of Espírito Santo, as partial requirement for obtaining a Master's Degree in Electrical Engineering.

Supervisor: Dr. Sc. Jair Adriano Lima Silva

Co-Supervisor: PhD. Marcelo Eduardo Vieira Segatto

FEDERAL UNIVERSITY OF ESPÍRITO SANTO - UFES
ELECTRICAL ENGINEERING POSTGRADUATE PROGRAM
Vitória-ES
2020

Menno Jan Faber

Performance Evaluation of the LoRa Wide Area Network Technology

Dissertation submitted to the Electrical Engineering Postgraduate Program of the Technological Center of the Federal University of Espírito Santo, as partial requirement for obtaining a Master's Degree in Electrical Engineering.

Approved on 17/07/2020, Vitória-ES.

Dr. Sc. Jair Adriano Lima Silva
Supervisor

PhD. Marcelo Eduardo Vieira Segatto
Co-Supervisor

D. Sc. Rodolfo da Silva Villaça
Examiner

D. Sc. Celso José Munaro
Examiner

D. Sc. Evandro Ottoni Teatini Salles
Examiner

FEDERAL UNIVERSITY OF ESPÍRITO SANTO - UFES
ELECTRICAL ENGINEERING POSTGRADUATE PROGRAM
Vitória-ES
2020

Ficha catalográfica disponibilizada pelo Sistema Integrado de Bibliotecas - SIBI/UFES e elaborada pelo autor

---

Faber, Menno Jan, 1985-
F115p Performance Evaluation of the LoRa Wide Area Network Technology / Menno Jan Faber. - 2020.
102 f. : il.

Orientador: Jair Adriano Lima Silva.
Coorientador: Marcelo Eduardo Vieira Segatto.
Dissertação (Mestrado em Engenharia Elétrica) - Universidade Federal do Espírito Santo, Centro Tecnológico.

1. Communication systems, Wireless. 2. Codificação. 3. Radiofrequência modulada. 4. Sistemas de telecomunicação. 5. Rádio - Interferência. 6. Comunicações digitais. I. Silva, Jair Adriano Lima. II. Segatto, Marcelo Eduardo Vieira. III. Universidade Federal do Espírito Santo. Centro Tecnológico. IV. Título.

CDU: 621.3

To the woman of my life, Keila, and to my parents, Jentsje and Janneke for their unconditional support at all times.

Acknowledgments

Firstly, to my Professors Dr. Jair Adriano Lima Silva and PhD. Marcelo Eduardo Vieira Segatto for the trust they placed in me and for the guidance and availability shown to solve the problems encountered.

To the Federal University of Espírito Santo (UFES) forgave me the opportunity to join the Master.

To all Professors of the Graduate Program in Electrical Engineering (PPGEE) at UFES, in particular, Professor Dr. Moises R. N. Ribeiro, Dr. Helder Rocha, and Dra. Maria José.

I also acknowledge the support from the project **NEsT-5G** (***N****úcleo de* ***Es****tudos em* ***T****ecnologias Emergentes para* ***5G***), which is supported in part by *Fundação de Amparo à Pesquisa e Inovação do Espírito Santo* and in part by *Conselho Nacional de Desenvolvimento Científico e Tecnológico.*

Special thanks to my fiancé Keila Christiane Nascimento for the affection, understanding, and support.

To my family, my parents and my brother and sister for the strength and understanding shown throughout my academic career.

To all my wonderful friends old and new, thanks for always being there for me!

To my colleagues at LabTel, researching the best ways to test and analyze the purpose of this work.

To the company 2Solve, especially Ricardo Calheiros Da Conceição and Klaas Minne Van Der Zwaag for their dedication, effort, and knowledge, making it possible to carry out this work.

Faraday is, and must always remain, the father of that enlarged science of electromagnetism. (James Clerk Maxwell)

Abstract

The Internet-of-Things (IoT) and Industry 4.0 markets will probably range amounts between $2.7 to $6.2 trillions by 2025, worldwide. In Brazil, these markets will generate $3.29 B by 2021. Wireless transmission techniques will play a significant role in these markets, despite the fact that most of the current wireless transmissions techniques are expensive and energy inefficient. One of the techniques that have become a front runner in such markets is long-range (LoRa). Beyond the robustness against interference, multipath fading, and the Doppler effect, LoRa is able to transmit over distances that can reach 10 Km in open areas and 3 Km in urban areas, at data rates that can reach 27 kbps. A theoretical study and an experimental evaluation of the performance of the LoRa technology are described in this work. Its performance in additive white Gaussian noise (AWGN) channels is addressed, through numerical simulations, to elucidate its communication capabilities in negative signal-to-noise ratio (SNR) conditions. Because of the importance of forward error correction (FEC) codes in the performance of modern systems, we propose an analytical bit-error-rate (BER) expression that considers the influence of the code rate parameter. The agreement between the theoretical and the numerical results of a Hamming coded system validated the proposed closed-form BER, evaluated in terms of SNR in AWGN channels.

Moreover, experimental setups with off-the-shelf LoRa wide area network (LoRaWan) equipment were prepared to demonstrate the feasibility of this promising technology, as well as the impact of the channel codification on the performance. Communication in urban and open areas with distances up to ≈ 3 and ≈ 10 km, respectively, were achieved, according to measurements of the average received signal indicators (RSSIs) around -100 dBm for an average SNR ≈ 5 dB. Additionally, feasible communication between a central oil-producing process used to monitor several oil wells, located in a rural area, was achieved at distances up to ≈ 2.7 km, according to measurements of the average RSSIs around -100 dBm for an average SNR ≈ 5.6 dB. It is possible to conclude from the experimental results that, LoRaWan is a suitable long-range and low power wide area network for smart monitoring in oil Industries.

Resumo

Estima-se que o mercado de internet das coisas e industria 4.0 alcançará cifras que se aproximarão dos $6,2$ trilhões de dólares em 2025, sendo que no Brasil este valor poderá alcançar $3,29$ bilhões em 2021. Sabe-se também que os sistemas de comunicação sem fio deterão papel fundamental neste promissor e necessário mercado. No entanto, boa parte das tecnologias que exploram tais sistemas não estão devidamente preparadas para abranger as demandas deste mercado devido, principalmente, a questões que envolvem custo de implantação e ineficiência no consumo de energia. É neste contexto que surge a tecnologia LoRa (*Long Range*) que além da robustez perante interferências, multipercurso e efeito Doppler, permite comunicações sem fio em um alcance de até 10 km à taxas de transferências que alcançam os 27 kbps. Um estudo teórico e uma avaliação experimental do desempenho da tecnologia LoRa são descritos neste trabalho, visando um melhor entendimento desta tecnologia de baixo consumo de potência.

Uma avaliação numérica do desempenho de um sistema LoRa em canais que adicionam ruído Gaussiano branco AWGN (*Adittive White Gaussian Noise*) permitiu elucidar seus recursos de comunicação em condições de relação sinal-ruído SNR (*Signal-to-Noise Ratio*) negativa. Devido à importância dos códigos de correção de erros, foi proposto uma expressão de taxa de erro de bits BER (*Bit-Error-Rate*) que considera a influência da taxa de codificação no desempenho. A concordância entre os resultados teóricos e os numéricos de um sistema com codificação Hamming validou a proposta em canais AWGN.

Além disso, sistemas LoRaWan (*Long Range Wide Area Network*) foram configuradas e instaladas com dispositivos disponíveis no mercado para demonstrar a viabilidade dessa tecnologia promissora, tanto em ambientes urbanos e suburbanos, bem como em um ambiente rural que simula a sua aplicação no monitoramento inteligente nas indústrias de petróleo. Comunicações em áreas urbanas e abertas com distâncias de até ≈ 3 e ≈ 10 km, respectivamente, foram alcançadas, mediante medições de RSSIs (*Received Signal Strength Indicators*) em torno de -100 dBm e com valores médios de SNR ≈ 5 dB. Além disso, a comunicação viável entre uma central de produção usada para monitorar vários poços de extração de petróleo, localizado em uma área rural, foi alcançada a distâncias de $\approx 2,7$ km, mediante valores RSSI em torno de -100 dBm e com valores de SNR ≈ 5.6 dB.

List of Figures

List of Tables

List of symbols

$\bar{b}$:	Message Words
B_W:	Signal Bandwidth
$\bar{c}_i$:	Code Words
CR:	Code Rate
C_{RX}:	Correlation Coefficient
d:	Distance
E_b/N_0:	Energy per bit to Noise Power Spectral Density
E_S:	Chirp Energy
f_c:	Center Operation frequency
f_{max}:	Frequency Maximum
f_{min}:	Frequency Minimum
f_{off}:	Frequency Offset
F_s:	Sampling Rate
G:	Generation Matrix
H:	Parity Check Matrix
$h(nT)$:	Impulse Response
h_{RX}:	Receiver Antenna Height
h_{TX}:	Transmitter Antenna Height
k:	Boltzmann constant
L:	Block Length
M:	Block of Transmitted Symbols
m:	Minimum distance
NF:	Noise Figure
N_oF:	Noise Floor

$\eta(nT)$: Zero mean Gaussian noise

P_{TX}: Transmitted Power

$PL_{Hata,O}$: Hata model Path Loss Open area

$PL_{Hata,SU}$: Hata model Path Loss Sub-Urban area

$PL_{Hata,U}$: Hata model Path Loss Urban area

R_S: Symbol Rate

$r_k(nT)$: Received LoRa Signals

R_b: Bit Rate

SF: Spreading Factor

$s_k(nT)$: Transmitted LoRa Signal

$s_i^*(nT)$: The complex conjugate of $s_k(nT)$

T: Sample Time

T_e: Temperature in Kelvin

T_{rx_delay1}: Delay before reception windows RX1

T_{rx_delay2}: Delay before reception windows RX2

T_S: Symbol Period

X_k: Data In

Y_k: Data Out

List of abbreviations and acronyms

ABP: Activation by Personalization

ADR: Adaptive Data Rate

AppEUI: Application Extended Unique Identifier

AppKey: Application Key

AppSKey: Application Session Key

AWGN: Additive White Gaussian Noise

BER: Bit-Error-Rate

BPSK: Binary Shift Keying

CSS: Chirp Spread Spectrum

dBm: decibel-milliwatts

dB: decibel

DevAddr: Device Address

DFT: Discrete Fourier transform

ECC: Error-Correcting Codes

ED: End-Device

EQ: Equalizer

FCntDown: Frame Counter Down

FCntUp: Frame Counter Up

FC: Frame Counter

FEC: Forward Error Correction

FFT: Fast Fourier Transform

GPRS: General Packet Radio Service

GPS: Global Positioning System

GW: Gateway

IFFT: Inverse Fast Fourier Transform

IIoT: Industrial Internet-of-Things

IoT: Internet-of-Things

ISM: Industrial, Scientific and Medical

LoRaWan: Long-Range Wide area network

LoRa: Long-Range

LOS: Line of Sight

LPWAN: Low-Power Wide-Area Network

MAC: Media Access Controller

MIC: Message Integrity Code

NLOS: Non Line of Sight

NwkSKey: Network Session Key

OA: Open Areas

OTAA: Over the air activation

PER: Packet Error Rate

PHY: Physical Layer

PL: Path Loss

PRBS: Pseudorandom Binary Sequences

RF: Radio frequency

RSSI: Received Signal Strength Indicator

RX1: Reception Window 1

RX2: Reception Window 2

SA: Suburban Areas

SF: Spreading Factor

SNR: Signal-to-Noise Ratio

SPI: Serial Peripheral Interface

TCP: Transmission Control Protocol

ToA: Time on-Air

TTN: The Things Network

UA: Urban Area

UDP: User Datagram Protocol

Contents

1 Introduction

A reindustrialization through the concept of Industry 4.0 is worldwide growing, also due to the rapid development of the information technology [Xu, He e Li 2014]. Industrial equipment in systems like transportation and manufacturing already demand, among others, intelligent communication and data processing through smart and low power networks [Qadir et al. 2018]. Indeed, long-range coverage, low data rates, energy efficiency, and cost-effective end-devices are important requirements attended by some low power wide areas network (LPWAN) technologies.

In its early stage, the Industrial Internet of Things (IIoT), that also belongs to the definition of dynamic network infrastructure with self-configuring capabilities, interoperable communication protocols, and virtual 'Things' identities, should be able to provide flexibility and scalability in future industrial networks such as transportation, healthcare environmental monitoring, production management, among others [Chen et al. 2018]. According to [Al-Fuqaha et al. 2015], the amount of Internet-connected devices will reach 212 billion in 2020, and by 2022, machine-to-machine communication will be responsible for 45% of the Internet traffic. Stimulating the application of Internet of Things (IoT) technology, these events obligate governments, enterprises, and academics to attend subjects like economic growth, business and scientific researches, respectively [Kuo et al. 2018]. It is speculated that by 2025 the IoT market value will range between $ 2.7 and $ 6.2 trillion [Al-Fuqaha et al. 2015].

Meanwhile, the 5th generation of mobile networks (5G) started to be deployed to provide ultra-reliable low-latency communication, as well as enhanced mobile broadband (eMBB) [Wunder et al. 2014]. The deployment of 5G networks operating at millimeter-waves, aiming eMBB use cases, imposes reductions in the link lengths [Yang et al. 2018]. To address the coverage drawback, mobile network operators (MNOs) are compelled to increase the number of base stations. Nevertheless, 5G can be considered, in use cases like massive machine-type communications (mMTC), as a backhaul for LPWANs applied in the context of IoT and Industry 4.0 [Yasmin et al. 2017], [Navarro-Ortiz et al. 2018]. The long-range and the low power consumption features, provided to the MNOs by the LPWANs, can be combined with scalability to be delivered by 5G, in order to attend both mMTC and eMBB. In such a scenario, the easy "anytime-anywhere" LPWAN deployment demonstrated in [Yasmin et al. 2017] can, indeed, provide new types of customers to traditional MNOs. Furthermore, according to the authors of [Navarro-Ortiz et al. 2018], operation and maintenance cost reductions, as well as additional end-to-end security can be ensured, if the MNOs infrastructure is utilized with a long-range wide area network (LoRaWan) gateway acting as a Node B.

Long-Range (LoRa) is a wireless narrowband technology using low cost and low power devices for low data rate transmission in ranges longer than traditional cellular networks, even with extremely low receiver sensitivity and signal detection with negative signal-to-noise ratios (SNRs) [AN1200.22 LoRa™ Modulation Basics 2015]. Commonly, it explores a kind of chirp spread spectrum (CSS) modulation technique that is robust against interference, multipath fading, and Doppler effect [Staniec e Kowal 2018]. In its turn, LoRaWan is the media access controller (MAC) layer protocol that uses LoRa as its physical (PHY) layer [Sørensen et al. 2017], [Reynders e Pollin 2016]. By employing multiple LoRaWan gateways, communicating through an Internet connection with a specific server, it is possible to build public and private wireless networks [AN1200.22 LoRa™ Modulation Basics 2015].

The continuous growth of the above-mentioned markets promoted the emergence of LPWAN technologies such as LoRaWan, Sigfox, Narrowband-IoT (NB-IoT), and Long-Term Evolution MTC (LTE-M) [Qadir et al. 2018], [Raza, Kulkarni e Sooriyabandara 2017]. Taking advantage of an already installed and mature infrastructure and, in theory, with better coverage [Lauridsen et al. 2017], NB-IoT and LTE-M has the disadvantage of operating in frequencies of the licensed bands. Low-cost deployment and short time-to-market are important advantages of LoRaWan and Sigfox, due to the use of owned licensed or license-free bands, like the industrial, scientific and medical (ISM) band [Raza, Kulkarni e Sooriyabandara 2017]. The fair coverage and capacity comparison between LoRaWan and Sigfox detailed in [Vejlgaard et al. 2017] shows that LoRaWan has better performance in outdoor environments with external interference.

1.1 Motivation

As above-mentioned, the total amount of Internet-connected devices will reach 212 billion in 2020 and will continue to grow exponentially. IoT and Industry 4.0 market on the edge of public implementation, with estimated values that will range between $ 2.7 trillion to $ 6.2 trillion by 2025, worldwide. The number of connected devices will be doubled by that time, and machine-to-machine communications will be responsible for 45% of the Internet traffic [Al-Fuqaha et al. 2015]. In Brazil, this market will generate $ 3.29B by 2021 [Estudo IoT na AL 2019 – Inter-American Development Bank 2019].

Wireless transmission techniques will play a significant role in these markets, but most of the wireless transmissions techniques that are used today, are expensive and energy inefficient. One of the techniques that have become a front runner in such markets is LoRa. Beyond the robustness against interference, multipath fading, and the Doppler effect, LoRa is able to transmit over distances that can reach 10 Km in open areas and 3 Km in urban areas, at data rates that can reach 27 kbps.

However, a better understanding of LoRa in the context of IoT and Industry 4.0 is necessary, in terms of practical measurements. Moreover, a better understanding of the impact of some physical (PHY) parameters, such as code rate, in the LoRa performance is also important. A straightforward comparison between numerical and analytic evaluations will certainly help the LoRaWan system designs.

1.2 Problem Definition and Justification

A history timeline shows that computer-based technologies, as well as those based on the internet and cellphones, significantly changed our lives. Nevertheless, there are still some important areas that can be improved, especially if the 5G context is taken into account. Smart cities, in which optimize empty parking spaces and by which traffic can be decreased, is an interesting example. Smart agricultural case, in which the moister in the soil is measured and irrigate can be turned on or off to save water, represents another scenario demanded nowadays. Among others, these are cases, in which IoT and Industry 4.0 can improve performances, enhance production processes, and at the same time, provide monetary gains. Wireless communication systems like LoRa can play an important role in these innovative technologies.

An in-depth study on the impact of PHY layer parameters, especially those related to the CSS modulation scheme and its respective demodulation process, can guide LoRa implementations in different kinds of areas and situations. Despite the fact that CSS is not a new modulation technique, it has only become popular in the last couple of years, also thanks to its adoption in the LoRa PHY layer. Even known that LoRa is a highly promising technology in a highly promising market, the amount of academic documentation about the effect of, for instance, the code rate, is still lacking. As a consequence, tools and models for performance evaluations in terms of numerical analytical simulations are still limited. The implementation of numerical models, to be used in LoRa transmission simulations, can provide an understanding of the robustness of such technology in IIoT environments? The model validation, through analytical models and experimental measurements from the real world, will surely assist the correct analysis of the LoRa´s amazing performance.

1.3 Objectives of this Work

The general objective of this research was to develop a numerical model to simulate LoRa/CSS modulation and compare this model with an analytic and real-world experiment, resulting in a better understanding of LoRa and its implementation. Special attention was reserved for performance analysis of LoRa systems in AWGN channels, considering the impact of the CR parameter.

To achieve the main objective, it was required to do an in-debt study on how the CSS modulation works, according to a design of a model used to simulate LoRa systems, and then compare the obtained results with analytical models and real-world experiments. Therefore, the specific objectives were:

- an in-debt study and implementation of the CSS modulation and demodulation;
- the development of a LoRa communication and its performance evaluation in AWGN and fading + AWGN channels;
- a comparison between numerical and analytical performance results;
- the configuration and the installation of a LoRa gateway in a LoRaWan;
- the execution of measurements in the LoRaWan at various locations and distances, considering parameters such as SNR and received signal strength intensity (RSSI);
- and a comparison between analytical results and real-world measurements.

1.4 Methodology

LoRaWan is discussed in numerous researches but the implementation of LoRa systems, with a focus on the performance of the CSS modulation format considering the impact of PHY layer parameters like CR, is not disseminated in the literature. Hence, an in-depth study about the main PHY layers parameters should be thoroughly considered, in order to comprehend the system completely. In the end, this will be responsible for leading the numerical and analytical simulations through different kinds of environments and situations. This bibliographic study demonstrates the exploratory nature of the research.

CSS signals are generated through software their performance in AWGN and fading channels are evaluated. The LoRa numerical model is validated through a comparison with theoretical BER closed-form previously proposed in the literature. A slight modification in the BER closed form is proposed to consider the effect of the code rate in the system performance. These tasks also corroborate with the explanatory nature of the evaluated numerical simulations.

Real-world data are acquired by creating a battery-powered LoRa node, that periodically transmit its GPS locations. The transmitted signals are received by a LoRa gateway installed on a high point in the Vitória metropolitan area, like “Convento da Penha” in Vila Velha. The gateway communicates, via the internet, to a LoRaWan network server, in which the received packets are stored. The interest was in the meta-data such as SNR, RSSI, GPS location, identifier, and uplink frame-counter (FCntUp), generated

at the reception of every LoRa message. Knowing the gateways and mobile LoRa node's location, it was possible to determine the distance of the communication.

During the experiment we made various measurements throughout the city at various locations, slowly increasing the distance between the gateway. The acquired data are analyzed and compared to values obtained by theoretical mathematical expressions, aiming the understanding of the LoRa robustness. These performance evaluations highlight the quantitative nature of the research.

1.5 Principal Contributions

In this work, we consider LoRa uplink systems in scenarios where the chirp spread spectrum is used as the modulation scheme. Focusing on the PHY layer, we evaluate the performance of such a system in AWGN channels, through numerical simulations. To elucidate the importance of FEC in the system performance, we proposed an analytical expression that considers the effect of the code rate on the BER metric. We demonstrate that the adoption of a Hamming code with high code rates introduces small penalties in the BER against signal-to-noise ratio, in detriment to a bit error correction in the signal detection that decreases the packet error rate (PER) metric.

Indeed, the impact of the CR parameter on the packet success rate was confirmed in an experimental setup implemented with off-the-shelf LoRaWan equipment to promote investigations that aims for a better understanding of the PHY layer mechanisms. In particular, the opposite behaviors perceived between the theory through BER and the experiments via PER could be explained by the simulations and experimental evaluations of the effect of the CR parameter. The agreement between the theory and the measurements attested the usefulness of such practical analysis in future system deployments.

Therefore, the contributions of this work include: (I) a closed-form expression for the BER versus SNR of a LoRa model that considers the impact of Hamming codification in AWGN channels; (II) an endorsement, through experimental analysis of received signal strength indicator, SNR and noise floor of the usefulness of the urban, suburban and open area channel models in future LoRaWan deployments and; (III) an experimental verification of the substantial impact of the parameter CR on the system PER. The main contributions of this work can be achieved in the following publications [1]:

C1 **Faber, M. J**; Zwaag, K. M. V. D.; Rocha, H. R. O.; Pereira E. da V.; Segatto, M. E. V.; Silva, Jair A. L., **Performance Evaluation of LoRaWan Applied to Smart Monitoring in Onshore Oil Industries**, in SBMO/IEEE MTT-S International Microwave and Optoelectronics Conference (IMOC), Aveiro, Portugal, 2019.

[1] Ci: Conference paper; Ji: Journal paper.

C2 Dos Santos, Willian G. V.; Costa, Wesley S.; **Faber, Menno J.**; Silva, Jair A. L.; Rocha, Helder R. O.; Segato, Marcelo E. V., **Sensor Allocation in a Hybrid Star-Mesh IoT Network using Genetic Algorithm and K-Medoids**, In: 2019 IEEE Latin American Conference on Communications (LATINCOM), Salvador, Brasil, 2019.

J1 **M. J. Faber**, K. M. v. Zwaag, W. G. V. Dos Santos, H. R. O. Rocha, M. E. V. Segatto and J. A. L. Silva, **A Theoretical and Experimental Evaluation on the Performance of LoRa Technology**, in IEEE Sensors Journal, 2020, doi: 10.1109/JSEN.2020.2987776.

It should be noticed that the research and the technological development described in this Dissertation are part of the subjects to be addressed in the project **NEsT-5G** (***N**úcleo de **Est**udos em **T**ecnologias Emergentes para **5G***) supported in part by *Fundação de Amparo à Pesquisa e Inovação do Espírito Santo* and in part by *Conselho Nacional de Desenvolvimento Científico e Tecnológico*.

1.6 Related Works

A bit-error-rate (BER) closed form of CSS in LoRa was estimated in [Reynders, Meert e Pollin 2016] from numerical simulations. The comparison with a binary-shift keying (BPSK) modulation scheme in additive white Gaussian noise (AWGN) channels shows that CSS based LoRa systems have a better performance. However, the proposed model only considers the effect of the spreading factor (SF) parameter. Meanwhile, in [Reynders e Pollin 2016] the authors provided a detailed study about the chirp spread spectrum in long-range systems. Their derived BER expression was evaluated through numerical simulations, from which they conclude that to achieve a BER $= 10^{-3}$, CSS based networks with a SF of 10 require 22 dB less power than those based on BPSK. Nevertheless, the authors did not consider the impact of channel coding in their investigations, as also, the rigorous mathematical derivations provided in [Vangelista 2017] and [Elshabrawy e Robert 2018]. The matched analytic and numerical results analyzed in both former publications also emphasize the robustness of CSS based LPWAN networks in AWGN and Rayleigh fading channels. In their conclusions, the authors of [Elshabrawy e Robert 2018] suggest the adoption of forward error correction (FEC) codes to decrease BER in LoRa transmissions over fading channels that characterizes urban environments.

The robustness of LoRa in the presence of high noise levels was demonstrated by the experimental results reported in [Angrisani et al. 2017]. The authors show that FEC can be important in packet loss reductions, despite its less impact, when compared to the effect of SF. However, an investigation aiming for a better understanding of the code rate

(CR) in BER analysis remained uncovered. A similar conclusion was obtained by the tree farm measurements described in [Yim et al. 2018]. The authors show that to maintain a reliable LoRa communication in such problematic areas, SF and CR should be configured in their highest values. In comparison with the present work, it should be stressed that they use a different metric (the packet delivery ratio) in their studies, which is important in the analysis of the impact of obstacles in the considered Fresnel zones.

To enhance the LoRa uplink performance, the authors of [Hoeller et al. 2018] proposed time and spatial diversities with message replication and multiple receive antennas, respectively. Their theoretical and numerical investigations show that the probability of reception increases in low-density networks. This strategy can be implemented in the practical scenario investigated in this work to decreases the packet error rate (PER), according to the employment of a code rate designed to reduce BER. At this point, it is important to refer to the straightforward relation between PER and BER derived in [Luvisotto et al. 2018] for indoor industry applications. Despite the confirmation that the probability of success depends on the number of end-devices, the authors of [Luvisotto et al. 2018] analytically show that, from a BER against signal-to-interference plus noise ratio, it is possible to estimate PER. It is worth noting that this procedure was not considered in the present work.

The analytic and simulation results presented in [Capuzzo, Magrin e Zanella 2018] prove that, when traffic grows excessively, the performance degrades in a LoRaWan cell. Realistic issues like adaptive data rate, duty cycle and multiple receive paths were addressed to exalt the advantages of LoRaWan. Evaluations considering such features can be conducted in the scenarios investigated in this work, according to specific adaptations.

1.7 Organization of this Dissertation

After a brief introduction to the topics under discussion, it is noteworthy to define the structure of the dissertation. Chapter 2 will lay out the theoretical background required for comprehending the analysis discussed throughout the text. The performance analysis of the implemented LoRa system is evaluated in Chapter 3, with an emphasis on the proposed BER closed-form and comparisons between numerical and analytical results. The LoRaWan basic concepts are defined in Chapter 4 and the experimental evaluations of LoRaWan in two different environments are described in Chapter 5. The concluding remarks are provided in Chapter 6.

2 LoRa Theoretical Background

Because of the robustness against noise interference, multipath fading, and Doppler effect provided by the modulation format, LoRa presents itself as a strong candidate for transmissions over a long distance, while being energy efficient [Reynders e Pollin 2016], [Staniec e Kowal 2018], [Farooq e Pesch 2018]. Therefore, low-cost devices are deployed in this wireless narrowband technology for low data rate transmission in ranges longer than traditional cellular networks, even with extremely low receiver sensitivity qwerty [AN1200.22 LoRa™ Modulation Basics 2015]. Usually operating in unlicensed bands, the chirp spread spectrum is considered as the modulation scheme used in the LoRa physical layer [AN1200.13 SX1272/3/6/7/8: LoRa Modem 2013]. The fundamentals of the LoRa physical layer model are described in this Chapter. In particular, the CSS modulation format, its performance in additive white Gaussian noise channels, and the urban and suburban channel models are mathematically described.

2.1 The CSS Modulation Format

Also known as frequency-shift chirp, the CSS generates chirp signals with a variable frequency that linearly increases or decreases over a certain amount of time, basically going from a minimum frequency (f_{min}) to a maximum (f_{max}), or in the opposite direction [AN1200.22 LoRa™ Modulation Basics 2015], [Vangelista 2017]. To modulate a symbol (a number of bits between 7 and 12) into a chirp, CSS uses a frequency offset f_{off} for every chirp, which is the start frequency of the chirp. The offset can be calculated by multiplying the symbol value with the symbol rate (R_s), which is obtained as $R_s = \frac{B_W}{2^{SF}}$, for B_W the signal bandwidth and SF the spreading factor. The frequency of the chirp increases until the higher bandwidth boundary (f_{max}), from which its value is cyclically shifted to lower boundary f_{min}. Again, the frequency increases, until it gets back to f_{off}, when the symbol completes one cycle. The time it takes to complete one chirp cycle is also denominated as symbol period $T_s = 2^{SF} \times T$, for $SF \in 7, 8, ...12$ and $T = 1/B_W$ a sample time, which is also known as chip.

With a chirp composed of 2^{SF} samples, a discrete-time LoRa symbol can be expressed as

$$\begin{aligned} s_k\left(nT\right) &= \sqrt{E_s} \times z_k\left(nT\right) \\ &= \sqrt{\frac{E_s}{2^{SF}}} \exp\left(j2\pi(k+n) \bmod 2^{SF} \cdot \frac{n}{2^{SF}}\right), \end{aligned} \tag{1}$$

for $k \in 0, 1, 2, ..., 2^{SF} - 1$, E_s the chirp energy, $s_k(nT)$ the basis functions of the signaling space and mod the modulo operator. It should be note that, in Eq. (1) the frequency offset expression $f_{off} = (B_W \times k)/2^{SF}$, as well as the symbol period and the sample time are considered as explained in [Elshabrawy e Robert 2018].

Considering the quasi-orthogonality of the chirp signals [Reynders e Pollin 2016], and supposing perfect time and frequency synchronizations after propagation in AWGN channels, the LoRa demodulation can be executed by the following correlation process

$$\sum_{n=0}^{2^{SF}-1} r_k(nT) \cdot s_i^*(nT) = \begin{cases} \sqrt{E_s} + \eta_i & i = k \\ \eta_i & i \neq k \end{cases} \tag{2}$$

where $r_k(nT) = s(nT) + \eta(nT)$ is the received waveform degraded by the zero mean white Gaussian noise $\eta(nT)$ of an AWGN channel and $s_i^*(nT)$ the complex conjugate of $s_k(nT)$ [Vangelista 2017]. According to [Elshabrawy e Robert 2018], [Seller e Sornin 2014] and [Georgiou e Raza 2017], the received symbol with highest correlation (obtained in the frequency domain with a fast Fourier transform) with the corresponded transmitted waveform can be detected as

$$Y_k = \arg_i \max \left(\left| \delta_{k,i} \sqrt{E_s} + \eta_i \right| \right), \tag{3}$$

in which $\delta_{k,i} = 1$ for $i = k$ and 0 otherwise.

2.2 Common LoRa Signal Bandwidths

In the older LoRa integrated circuits, there are only three possible signal bandwidths to select, which are 125, 250, and 500 KHz [SX1276/77/78/79 - 137 MHz to 1020 MHz Low Power Long Range Transceiver 2019]. In the new versions of LoRa, it is possible to adopt one of 11 possible signal bandwidths, with the lowest value being 7.8 kHz and the highest 500 kHz [SX1272/73 - 860 MHz to 1020 MHz Low Power Long Range Transceiver 2015]. Nevertheless, in the case of LoRaWan, the possible selectable signal bandwidths are limited to 125, 250, and 500 kHz.

2.3 LoRa Spreading Factor

The spreading factor (SF) is a important parameter in LoRa systems and can be configured to have a value between 7 and 12. It is responsible for the time the CSS format takes to complete one LoRa symbol or a chirp. This symbol period can be expressed as $T_s = \frac{2^{SF}}{B_w}$ [AN1200.22 LoRa™ Modulation Basics 2015]. The symbol period has a big impact on the bit rate of the LoRa system, and on the sensitivity of the LoRa receiver. This introduces a trade-off that must be take into account when a LoRa system is designed.

Table 1 shows a comparison between bit rate (R_b), symbol period (T_s) and receiver sensitivity [1]. The bit rate can be expressed as $R_b = SF \cdot \left(\frac{B_w}{2^{SF}}\right) \cdot \left(\frac{4}{4+CR}\right)$, for CR the code rate.

Table 1 – Spreading factor trade-off considering that $CR = 1$.

SF	R_b **in kb/s**	T_s **in ms**	**Sensitivity in dBm**
7	6.836	1.0	−123
8	3.906	2.0	−126
9	2.197	4.1	−129
10	1.221	8.2	−132
11	0.672	16.4	−134.5
12	0.366	32.8	−137

It can be clearly seen in Table 1 that, with every increment of SF, the receiver sensitivity improves 3 dB, with total improvement of 14 dB for $SF = 12$ over $SF = 7$. However, every increment of SF doubles the symbol period and, as a consequence, halves the system bit rate. With $SF = 7$ the system takes 1 ms to transmit one chirp with a corresponding bit rate of 6.836 kb/s, while for $SF = 12$ it takes 32.8 ms at 0.366 kb/s. It is worth noting that the amount of bits that represents a chirp is determined by SF, which means that, for a LoRa signal with $SF = 7$ one chirp is composed of 7 bits, whereas for $SF = 12$ the chirp represents 12 bits.

2.4 LoRa Forward Error Correction

The amount of noise in LoRa can decrease communication reliability through packet loss. In this context, channel coding becomes fundamental to overcome the effect of channel noise. With FEC techniques, modern communication systems typically add controlled redundancy in the data sequence to detect and, until certain limits, correct errors that may occur during the transmission [Wells 1998]. This is also known as error-correcting codes (ECC) and can be classified in block codes and convolutional codes. A block code is linear if the sum of two codewords is also a code word ($\bar{c}_i$). Furthermore, if a block of transmitted symbols is composed of the elements of an alphabet $M = \{0, 1\}$, the ECC is called a binary error-correcting code.

As a binary ECC, the Hamming codes belong to the family of single error-correcting codes with a block length $L = 2^m - 1$, for $m \geq 3$ (minimum distance). Thus, the data source is organized in blocks of $k = 2^m - m - 1$ bits as $\bar{b} = b_0, b_1, ..., b_{k-1}$ message words,

[1] Value are obtained from [AN1200.22 LoRa™ Modulation Basics 2015]

before codification in codewords $\bar{c} = c_0, c_1, ..., c_{L-1}$ of length L. For Hamming (7,4), a message word of four bits is encoded in a code word of 7 bits, in which the three parity bits that are added can be obtained as

$$p_1 = b_1 \bigotimes b_2 \bigotimes b_4,$$
$$p_2 = b_1 \bigotimes b_3 \bigotimes b_4,$$
$$p_3 = b_2 \bigotimes b_3 \bigotimes b_4.$$

The XOR operator is used in the covered message bits and, during the determination of the parity bits, the parity bit is set to zero if the sum of the covered bits is odd, and set to one if the sum is even. The Parity-bit-generator matrix of Hamming (7,4) can be found as,

$$\mathbf{P} = \begin{bmatrix} 1 & 1 & 0 \\ 1 & 0 & 1 \\ 0 & 1 & 1 \\ 1 & 1 & 1 \end{bmatrix}, \tag{4}$$

where the columns represent the parity bits and the rows the bits that are covered in the message word. The first column represents the parity bit p_1, covered by bits b_1, b_2 and b_4 represented by one´s. Because b_3 is not covered its value is zero. From the matrix $\mathbf{P}$, the generator matrix $\mathbf{G}$ can found as

$$\mathbf{G} = [\mathbf{P}|\mathbf{I}], \tag{5}$$

in which $\mathbf{I}$ is the identity matrix. With the generator matrix, the message word can be encoded in the codeword as follows,

$$\bar{b}\mathbf{G} = \bar{c}. \tag{6}$$

To decode the codewords $\bar{c}$, the following parity-check matrix $\mathbf{H}$ is needed,

$$\mathbf{H} = \left[\mathbf{I}|\mathbf{P}^T\right], \tag{7}$$

where $\mathbf{P}$ is the above-mentioned parity-bit-generator matrix and $\mathbf{I}$ is the identity matrix. With parity-check matrix, the codeword can be decoded as

$$\mathbf{H}\bar{c}^T = \bar{z} \tag{8}$$

for $\bar{z}$ a syndrome vector that identifies if an error occurred and for which codeword bit it occurred. If the syndrome vector is composed only by zeros, no error is detected. However, if the syndrome vector is not zero there is an error in the code word. The erroneous bit is the column position from the parity-check matrix that matches the syndrome vector. The erroneous bit can then be corrected and the original message word recovered.

2.5 System Performance in AWGN Channels

To confirm the accuracy of numerical models, it is extremely important to adopt an analytic expression for the BER performance of the simulated LoRa system in AWGN channels. The approximations presented in [Reynders, Meert e Pollin 2016] and [Elshabrawy e Robert 2018] are two important BER performances of LoRa modulation found in the literature. However, both expressions (see equations (23) and (24) of Ref. [Elshabrawy e Robert 2018]) do not consider the impact of the code rate parameter in the aforementioned performance. Hence, one of the main contribution of this work outcome from a modification proposed in the following BER expression

$$\text{BER} = Q\left(\frac{\log_{12}(SF)}{\sqrt{2}} \cdot \frac{E_b}{N_0}\right), \tag{9}$$

in which the Q function, that is closely related to Gaussian random variables, is defined as $Q(x) = \frac{1}{\sqrt{2\pi}} \int_x^\infty e^{-\frac{t^2}{2}} dt$. The E_b/N_0 parameter represents the energy per bit to noise power spectral density [Reynders, Meert e Pollin 2016] calculated as following

$$\frac{E_b}{N_0}\,[\text{dB}] = \text{SNR}\,[\text{dB}] + 10\log_{10}\left(\frac{B_W}{R_b}\right)[\text{dB}]\,, \tag{10}$$

for SNR a pre-defined signal-to-noise ratio in an AWGN channel and dB the decibel logarithmic unit [Jun et al. 2017]. It is clear from Eq. (9) that the BER decreases with the E_b/N_0 and the SF parameters. It is important to note that increments in SF increases the symbol period and, as a consequence, decreases the system bit rate. Neglecting channel coding, the bit rate shown in equation (10) is defined as $R_b = SF \cdot \frac{B_w}{2^{SF}}$ in b/s [Reynders e Pollin 2016], [Reynders, Meert e Pollin 2016]. Nevertheless, considering a channel coding at a rate $\frac{4}{4+CR}$, the useful bit rate is $R_b = SF \cdot \left(\frac{B_w}{2^{SF}}\right) \cdot \left(\frac{4}{4+CR}\right)$, for CR the code rate defined in [AN1200.22 LoRa™ Modulation Basics 2015], [Augustin et al. 2016].

The received signal strength indicator is an important measurement parameter that reflects the quality of LoRaWan links [AN1200.13 SX1272/3/6/7/8: LoRa Modem 2013]. For NF the receiver noise figure and P_{TX} the transmitted power, it is possible to estimate the SNR from measured values of RSSI as following

$$\text{SNR}\,[\text{dB}] = \text{RSSI} - P_{TX} + 174 - 10 \times \log_{10}(B_W) - NF. \tag{11}$$

2.6 Urban, Suburban and Open Area Channel Models

As a wireless communication system, the performance of LoRa is mainly governed by the wireless channel environment. Classified as a large-scale fading channel, path loss (PL) and shadowing by large objects are important sources of signal degradation [Park, Chen e Choo 2017]. The Hata model is one of the most popular used to calculate path loss for microwave radio links up to 1500 MHz and 100 Km [Park, Chen e Choo 2017]. As

an extension of the Okumura model, it covers multiple different environments, including Urban, Suburban, and Open areas. According to the Hata model, the path loss for a certain distance d (in meters) in Urban areas can be calculated as

$$\begin{aligned} PL_{Hata,U}(d)[\text{dB}] = 69.55 \\ + 26.16 \times \log_{10}(f_c) \\ - 13.82 \times \log_{10}(h_{TX}) \\ - C_{RX} \\ + 44.9 \times \log_{10}(d) \\ - [6.55 \times \log_{10}(h_{TX})] \times \log_{10}(d) \end{aligned} \tag{12}$$

for f_c the operation center frequency in MHz, h_{TX} the transmitter antenna height in meters, and h_{RX} the height of the receiver antenna. For small to medium-sized coverage, the correlation coefficient C_{RX} of the receiver antenna is given as

$$C_{RX} = 0.8 + [1.1 \times \log_{10}(f_c) - 0.7]\, h_{RX} - 1.56 \times \log_{10}(f_c), \tag{13}$$

while for larger coverage it is achieved as

$$C_{RX} = \begin{cases} 8.29\Big[\log_{10}(1.54 \times h_{RX})\Big]^2 - 1.1, \text{ if } 150 \leq f_c \leq 200 \text{ MHz} \\ 3.20\Big[\log_{10}(11.75 \times h_{RX})\Big]^2 - 4.97, \text{ if } 200 \leq f_c \leq 1500 \text{ MHz}. \end{cases} \tag{14}$$

Moreover, for suburban ($PL_{Hata,SU}$) and open ($PL_{Hata,O}$) areas, the path loss can be obtained as

$$PL_{Hata,SU}(d)[\text{dB}] = PL_{Hata,U}(d) - 2\left[\log_{10}(f_c/28)\right]^2 - 5.4, \tag{15}$$

$$\begin{aligned} PL_{Hata,O}(d)[\text{dB}] = PL_{Hata,U}(d) \\ - 4.78 \times [\log_{10}(f_c)]^2 \\ + 18.33 \log_{10}(f_c) \\ - 40.94. \end{aligned} \tag{16}$$

2.7 Determination of the Noise Floor

A LoRa receiver is able to receive a signal under the noise floor down to -20 dBm, when configured with a bandwidth of 125 kHz and an SF of 12 [AN1200.13 SX1272/3/6/7/8: LoRa Modem 2013]. Nevertheless, it depends on variables like location, temperature, front end circuit, among others. To correctly determine the receiver sensitivity, it is crucial to know the noise floor N_oF, that can be obtained as

$$N_oF = 10 \times \log_{10}(k \times T \times B_W) + NF \text{ [dBm]}, \tag{17}$$

where k is the Boltzmann constant, T_e the temperature in Kelvin, NF is the noise figure of the front end circuit [AN1200.22 LoRa™ Modulation Basics 2015].

3 Performance Analysis of LoRa Systems

The numerical models and the analytical expressions used to evaluate the performance of LoRa systems are described in this Chapter. A performance comparison between the models and the mathematical expressions gives a clear inside in the robustness of the CSS modulation scheme in the LoRa physical layer. The simulation results obtained in terms of BER against SNR in AWGN and fading channels are also outlined. Furthermore, a proposal of a new BER closed-form, which considers the impact of FEC in the performances, is introduced and its accuracy confirmed through simulations.

3.1 The Numerical Models used in the Simulations

Fig. 1 shows a block diagram of the numerical model used to simulate and evaluate the performance of a LoRa communication system through AWGN and frequency-selective channels [All About LoRa and LoRaWAN]. Pseudorandom binary sequences (PRBS) are divided into sub-sequences of SF bits before symbol mapping in x_k integers between 0 and 2^{SF}. Then, the symbols are used to modulate a varying central frequency electrical carrier in the chirp generating sub-block, i.e., the $s_k(nT)$ modulated signals of equation (1) are generated according to the CSS modulation format described in Section 2.1.

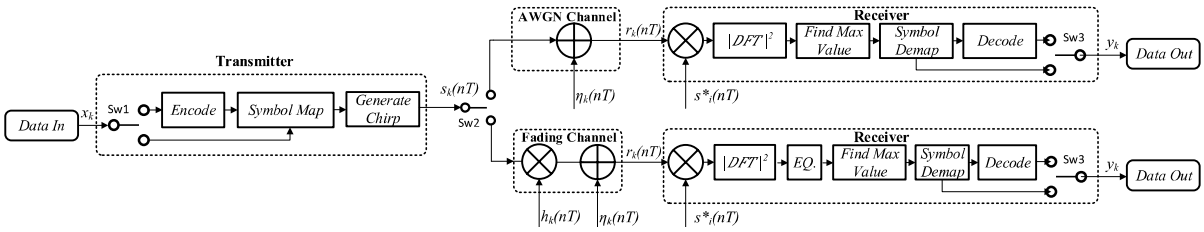

Figure 1 – LoRa simulation model. *Map*: mapping; $|DFT|^2$: square of the absolute value of the discrete Fourier transform; *EQ*: Equalizer; *Demap*: demapping. The fading channel $h(nT)$ is modeled as a statistical Rayleigh channel.

After propagation through the evaluated channels, the received LoRa signals $r_k(nT)$ are convoluted with $s_i^*(nT)$, a complex conjugate of the basis function $s_k(nT)$. It is important to notice that the AWGN channel adds the zero mean Gaussian noise $\eta(nT)$, and the frequency-selective channel is modeled as a Rayleigh fading channel with an impulsive response given by $h(nT)$ [Staniec e Kowal 2018], [Proakis e Salehi 2008].

The symbol detection used in the model is based on the frequency domain method shown in Fig. 1. After processing the square value of the absolute value of the discrete

Fourier transform ($|DFT|^2$) on the convoluted data chirps, the symbols are detected through a maximum value calculation process. In the case of propagation through the fading channel, a frequency domain equalizer (EQ) [1] is applied to overcome the frequency-selective effects provided by multipath. The detected bits are obtained after conventional de-mapping processing. It should be stressed that an $|DFT|^2$ process occurs at each chirp duration, that is, with a length of 2^{SF} samples. It is also important to emphasize that the position of the detected maximum sample corresponds to the symbol values.

3.2 Examples of Generated and Detected Signals

Fig. 2 shows an illustrative example of the generated signals $s_k(nT)$ in a time *versus* frequency plot. The first 8 chirps are used as a preamble and have a symbol value of 0, which means that the chirps starting at the lower boundary f_{min} and linearly increase to the higher boundary f_{max} of the bandwidth. Used at the receiver for synchronization, the next two chirps are inverse chirps, when compared to the preamble and data chirps, as they start at the higher boundary and linearly decrease to f_{min}.

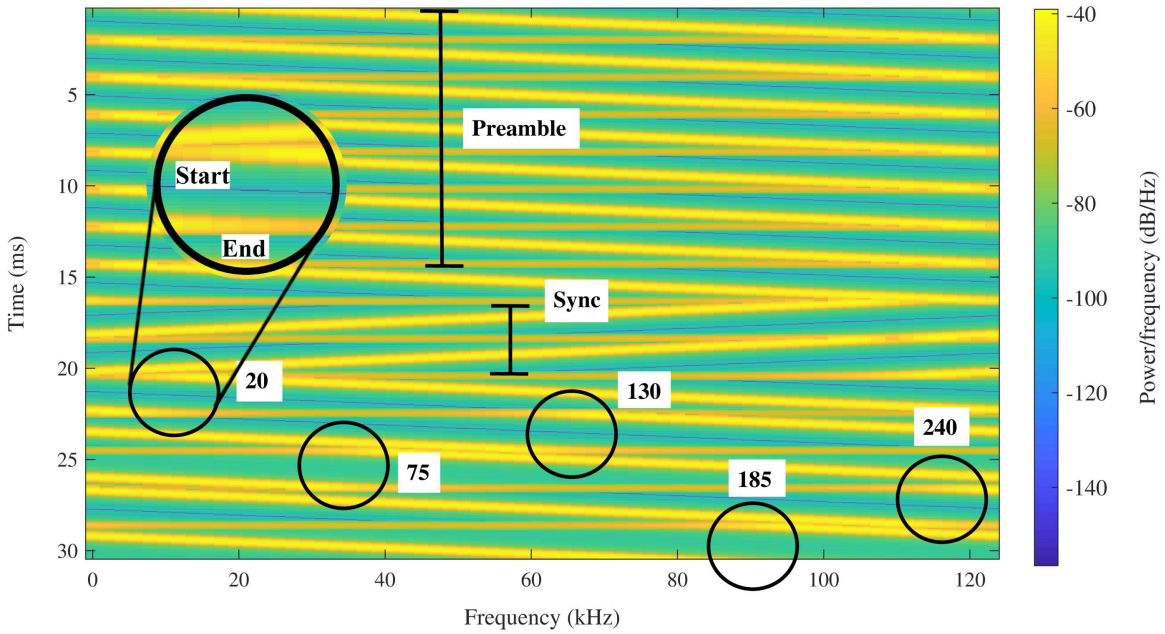

Figure 2 – Time *versus* frequency plot of part of the generated $s_k(nT)$ modulated signals, with $SF = 8$ and $B_w = 125$ kHz.

Frequency shifts (jumps) in the data chirps are clearly depicted in Fig. 2. The frequency offset f_{off} can be calculated by multiplying the symbol value with the symbol rate R_s. For the symbol value of 20, the f_{off} is equal to 9.765 kHz, as verified in Fig. 2.

[1] We choose a one-tap equalizer due to complexity reduction. We also consider a perfect channel recognition for the sake of simplicity.

Fig. 3 shows an illustrative example of generated $s_i^*(nT)$ signals, the complex conjugate of $s_k(nT)$, in a time *versus* frequency plot [Vangelista 2017]. Similar to the synchronisation chirps, they are the inverse of the data chirps. The $s_i^*(nT)$ signals are generated at the receiver side and are used in the complex convolutions with $r_k(nT)$, that, for the considered example, generate the result depicted in Fig. 4.

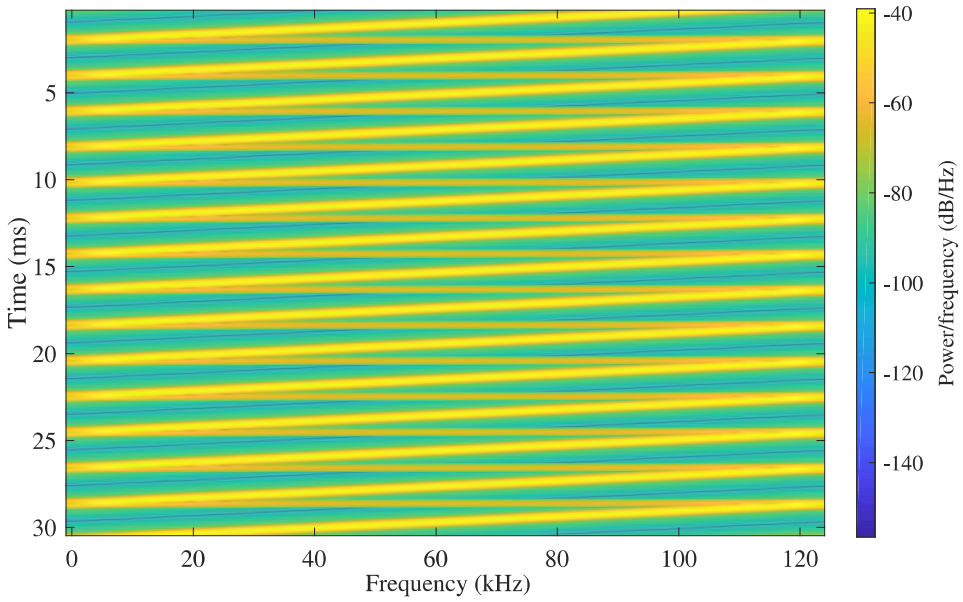

Figure 3 – Time *versus* frequency of part of the generated $s_i^*(nT)$ modulated signals, with $SF = 8$ and $B_w = 125$ kHz.

It can be verified from the convolution resultant $r_k(nT)$ signals, shown in Fig. 4, that the data chirps energy (E_s) are clearly depicted, after the synchronization with downchirps [see Eq. (2)]. It is clear that the energy of the data chirps is considerably higher than those of its surroundings. The energy of the preamble (the 8 data chirps with a symbol value of 0) is concentrated on the left side of Fig. 4, whereas the energy of the two synchronization chirps is uniformly spread over the bandwidth. The 9.765 kHz offset associated with the above-mentioned symbol 20 becomes clear, back in Fig. 4.

Fig. 5 shows a result similar to that shown in Fig. 4, however, with a system SNR$= -10$ dB. The result shows that, even in a high-intensity noise scenario, the data chirps can be recovered from the received signal. It should be noticed that, in practical LoRa implementations, the data chirps can be decoded in a system with SNR$= -20$ dB, if a $SF = 12$ and 125 kHz bandwidth are employed [AN1200.13 SX1272/3/6/7/8: LoRa Modem 2013].

In order to briefly demonstrate the robustness against interference, we transmitted a LoRa signal with an interfering signal generated with a $SF = 7$ [Staniec e Kowal 2018]. Fig. 6.(a) shows the resultant received signal, before the complex convolution. It is clear in this case that, unlike the one shown in Fig. 2, it gets increasingly difficult to see the symbols.

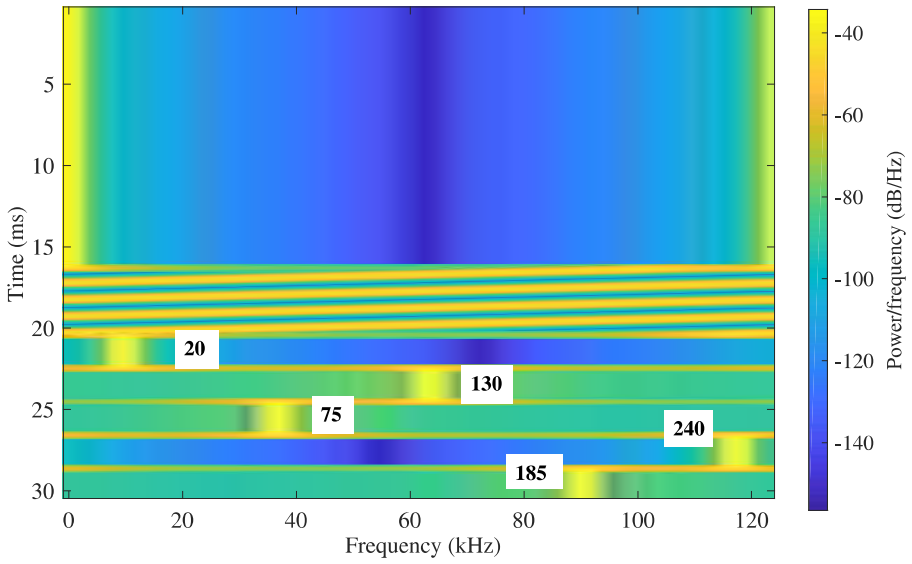

Figure 4 – Time *versus* frequency of part of the signals $r_k(nT)$ received in a back-to-back configuration, and after the complex convoluted with $s_i^*(nT)$.

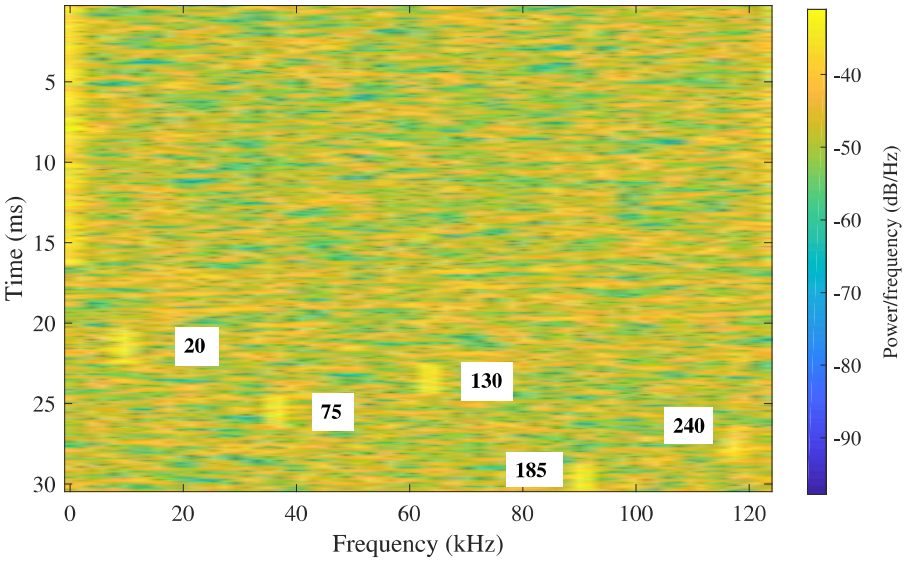

Figure 5 – Time *versus* frequency of part of the received $r_k(nT)$ signals, after the complex convoluted with $s_i^*(nT)$, considering an SNR= -10 dB.

The result of the complex convolution $r_k(nT)$ is shown in Fig. 6.(b). It can be noticed that because of the interfering signal, the result is much less clear than the result depicted in Fig. 4. Nevertheless, the data recovering is still possible due to the quasi-orthogonality of LoRa systems [Reynders e Pollin 2016]. The energy of the interfering LoRa signal is uniformly spread over the chirps bandwidth, and thus introduces little impact in the symbol values recover at the receiver. However, it needs to be disclosed that, interfering LoRa signals with the same spreading factor provides destructive collisions [Reynders e Pollin 2016].

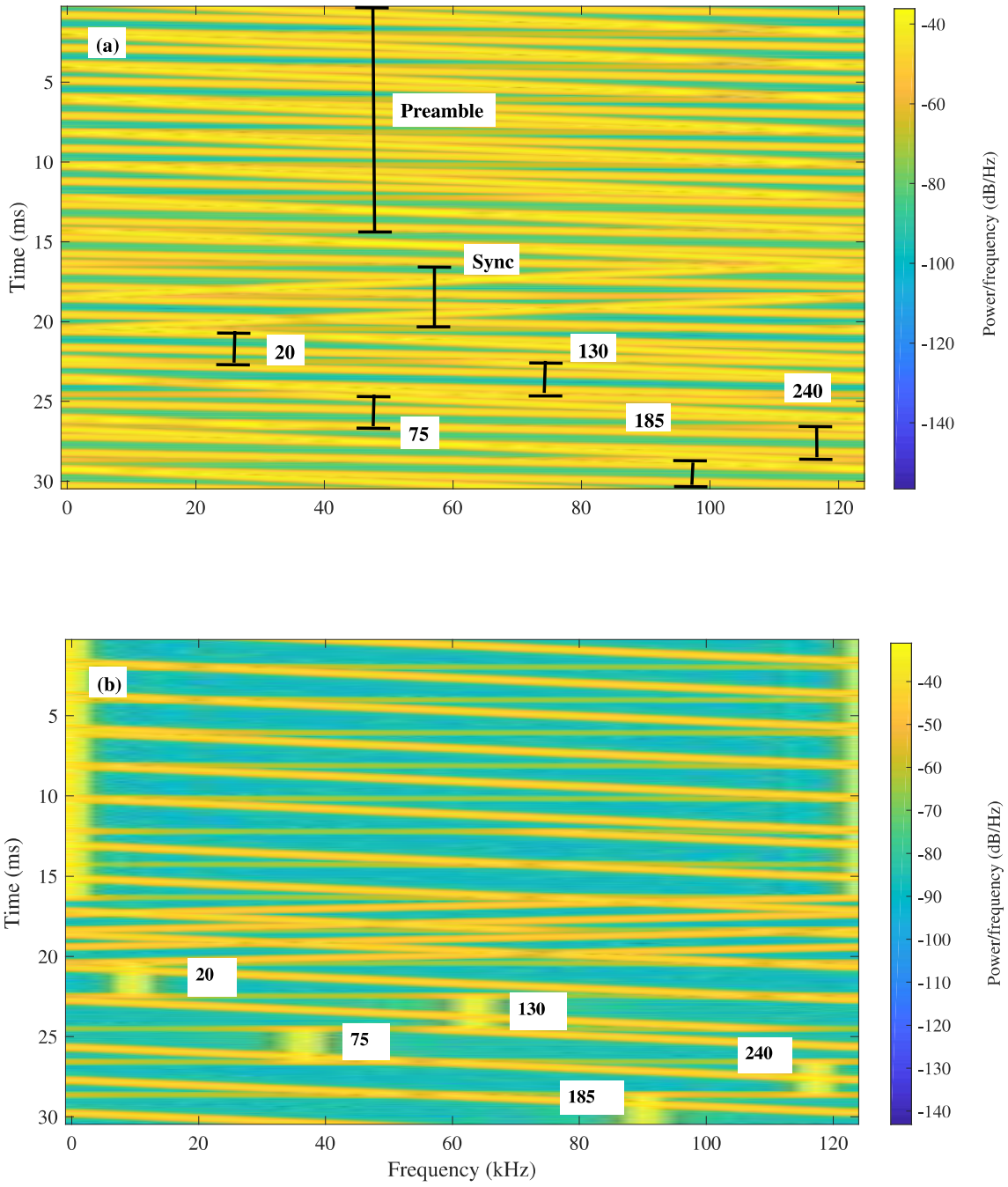

Figure 6 – (a) Time *versus* frequency plot of part of the generated $r_k(nT)$ modulated signals, with $SF = 8$ and $B_w = 125$ kHz. Including a interfering LoRa Signal, with $SF = 7$. (b) Time *versus* frequency of part of the received $r_k(nT)$ signals, after the complex convoluted with $s_i^*(nT)$.

3.3 Example of Data Recovering

To illustrate the data recovering process, consider the part of the diagram, depicted in Fig. 1, used to detect signals corrupted by AWGN. Fig. 7.(a) shows the detected symbols in a system back-to-back [2] configuration, for comparison purposes. The symbols were obtained after an $|DFT|^2$ process accomplished in the $r_k(nT)$. It should be stressed that the $|DFT|^2$ was taken separately over every data chirp with a length of 2^{SF} samples.

It can be verified in Fig. 7. (a) that the results of an $|DFT|^2$ process are a sharp spike at the position where E_s is the highest. The recovered data symbol is its corresponding value in the x axis of the $|DFT|^2$ (see the value 20 of the aforementioned example). It can be seen from Fig. 7.(b) that the symbols are also correctly detected after propagation in an AWGN channel with a SNR= -10 dB. The symbols with value 20 are clearly detected even with such low SNR, despite the variable $|DFT|^2$ amplitudes occurred in this case.

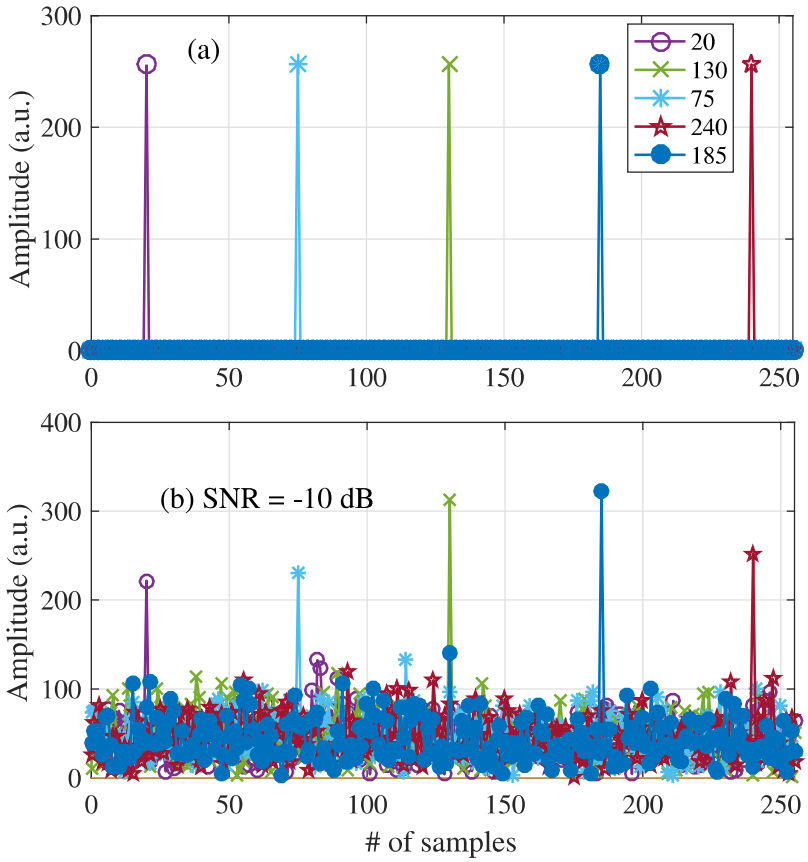

Figure 7 – Amplitude unit (a.u) of the detected symbols after (a) back-to-back and (b) AWGN channel with SNR= -10 dB.

[2] No noise is added in this configuration, which means that the receiver input is exactly the same as the transmitter output.

3.4 Performance Analysis of LoRa in AWGN Channels

In order to evaluate the performance of the numerical model depicted in Fig. 1, we conduct Monte Carlo Simulations of the CSS LoRa based system under the effect of AWGN channels. The simulation results obtained with the numerical model are compared with the theoretical BER expression given by Eq. (9). Table 2 summarizes the parameters used to generate the CSS signals.

Table 2 – System parameters for AWGN channel evaluation.

Parameter	**Symbol**	**Value**	**Unit**
PRBS	-	$4 \times (2^9 - 1)$	bits
Bandwidth	B_W	125	kHz
Spreading factor	SF	7, 10, 12	-
Code rate	CR	1, 2, 3, 4	-
Bit rate	R_b	183, 5418	b/s
Sampling rate	F_s	125	kS/s
Preamble length	-	8	symbols
Sync length	-	2	symbols

Fig. 8 shows the BER system performance as a function of different values of SNR quantified in terms of the energy per bit to noise power spectral density ratio E_b/N_0. As expected, the performance strongly depends on the spreading factor [AN1200.22 LoRa™ Modulation Basics 2015]. It can be seen from Fig. 8 that, for $SF = 12$, a BER $= 10^{-5}$ can be reached with an E_b/N_0 of 7.8 dB, while for $SF = 10$ and 7 this performance is achieved with $Eb/N0$ equal to 8 and 9 dB respectively.

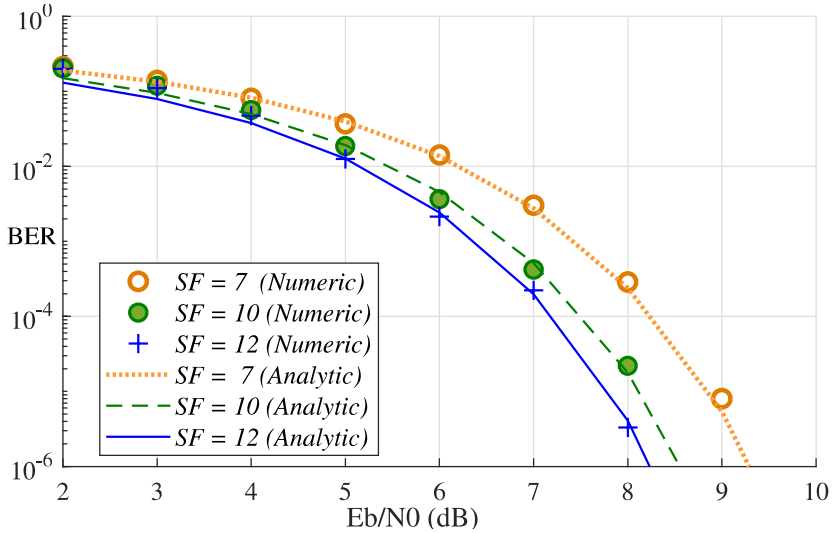

Figure 8 – BER *versus* E_b/N_0 for $SF = 7$, 10 and 12, with $CR = 4$.

It is clear from Fig. 8 that, the simulation results follow the analytic model given by equation (9) with the SF considered in the numerical simulations. Hence, we conclude that the agreement between the theoretical and the numerical results validate the implemented numerical model, in LoRa systems with a PHY layer without channel coding.

3.5 The Proposal of a new BER Closed-Form

The numerical model and the analytical expression of Eq. (9) does not consider error correction, which plays an important role in packet loss. Therefore, in order to evaluate the impact of FEC in the LoRa PHY layer, we propose the following BER expression,

$$\text{BER} = Q\left(\frac{2 \cdot \log_{12}(SF) \cdot \left(\frac{4}{4+CR}\right)}{\sqrt{2}} \cdot \frac{E_b}{N_0}\right). \tag{18}$$

The expression provided in (18) was achieved by mathematical intuition, considering several BER close expressions that considers the channel coding [Proakis e Salehi 2008], [Wells 1998]. It is also straightforward to infer the location of the code rate in the expression due to the direct relation between the SF parameter and the information bits.

According to [Seller e Sornin 2014], a code rate factor of $\frac{4}{4+CR}$ is preferable when Hamming code is used as the FEC technique in LoRaWan. This factor represents a SNR penalty if it is directly multiplied by the $\frac{E_b}{N_0}$ parameter in the equation (18). The incorporation of this parameter is imperative in the analysis that considers multipath channels like the packet error rate measurements described in [Staniec e Kowal 2018]. To emphasize the importance of the modification in the BER system performance (see Eq. 18) we also conducted simulations with different values of code rate. Fig. 9 shows the BER performance against E_b/N_0 considering $CR = 1, 2, 3$ and 4, where $CR = m$.

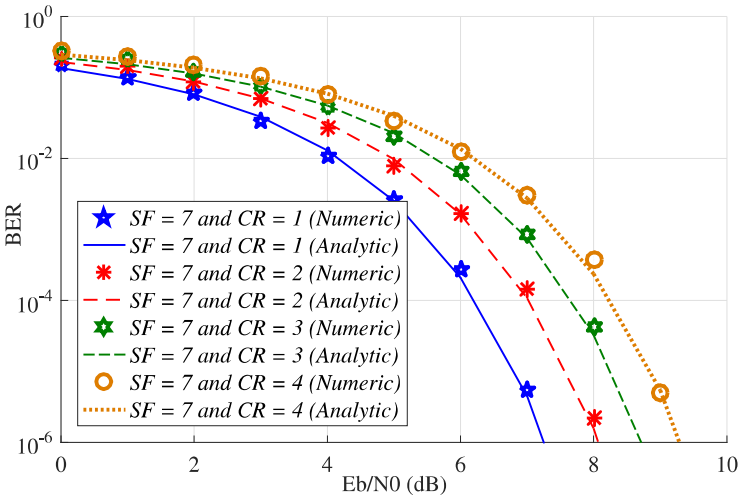

Figure 9 – BER *versus* E_b/N_0 for $CR = 1, 2, 3$ and 4, with $SF = 7$.

It can be observed from Fig. 9 that the performance depends on the selected CR. The system performance decreases with unit increments in the CR. This can be explained with a close look at Eq. (18) where an increase in the CR provides a deterioration in the factor that multiplies the E_b/N_0, thus rising the BER. A BER $= 10^{-5}$ is achieved with $E_b/N_0 = 6.83, 7.62, 8.29$ and 8.87 dB, for code rates equal to $1, 2, 3$ and 4, respectively. Therefore, in a practical design where increases in the SF are prohibitive, the system performance can be enhanced, decreasing the CR.

It is also clear in Fig. 9 that, the simulation results follow the analytic expression given by equation (18) with the $SF = 7$, validating the BER modification proposed in [Faber et al. 2020]. Both numerical and analytic results depicted in Fig. 9 were obtained considering the fact that a modification in the CR alters the useful bit rate and, in consequence, the E_b/N_0 and hence the bit error rate. However, to analyze the effect of FEC in the numerical model, channel coding should be considered. Thus, due to the recommendation provided in [Seller e Sornin 2014], a Hamming code at a rate $\frac{4}{7}$ ($CR = 3$) was implemented in the numerical model by switching Sw1 and Sw3 in Fig. 1 towards encoding and decoding, respectively. For the sake of comparison, we also conduct simulation with a coded system at a code rate of $\frac{4}{5}$ ($CR = 1$).

Fig. 10 shows performance comparisons between the systems at code rates of 1 and 3 in AWGN channels. It is observed that increases in CR also increase BER, which is explained by the redundant bits introduced by the codification that demands a higher value of E_b/N_0 to achieve the same BER. Fig. The agreement between the analytic results provided by Eq. (18) and those obtained by the coded numerical models, in both examined values of CR, validates the proposed BER expression.

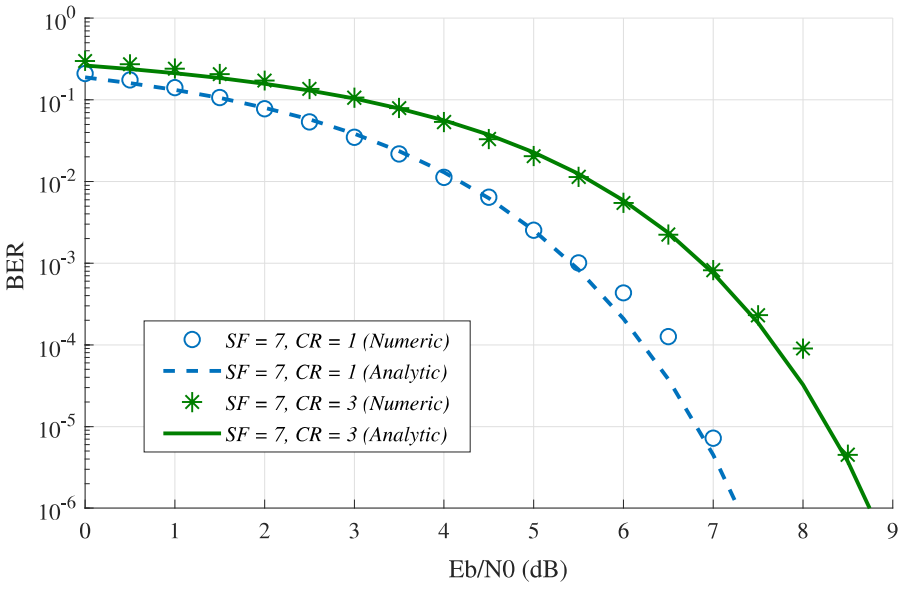

Figure 10 – BER *versus* E_b/N_0 for coded systems with $CR = 1$ and 3 in AWGN channels.

3.6 Performance Analysis of LoRa in Fading Channels

To evaluate the impact of frequency selectivity of practical environments, we also investigate the influence of multipath fading according to propagation through frequency-selective fading channels. Fig. 11 shows performance comparisons between coded systems for code rates of 1 and 3. The analytical performance in AWGN channels is also shown for comparisons. Table 3 summarizes the parameters used to generate the CSS signals.

Table 3 – System parameters for Fading channel evaluations.

Parameter	**Symbol**	**Value**	**Unit**
PRBS	-	$4 \times (2^9 - 1)$	bits
Bandwidth	B_W	125	kHz
Spreading factor	SF	7	-
Code rate	CR	1, 3	-
Impulsive response	$h(nT)$	2	-
Sampling rate	F_s	125	kS/s
Preamble length	-	8	symbols
Sync length	-	2	symbols

The frequency-selective channel is modeled as a Rayleigh fading channel with an impulsive response given by $h(nT)$ with two taps. An equalization process, provided by a single tap equalizer, was implemented after the FFT to overcome the effect of the frequency selectivity introduced by such fading channels [Cho et al. 2010]. A performance penalty of ≈ 3 dB is observed at a BER $= 10^{-4}$ (compared to the AWGN performance) illustrates the above-mentioned impact. Furthermore, Fig. 11 also shows that, as expected, the codification does not influence the system performance, unlike the equalization process that is mandatory in such type of propagation [Proakis e Salehi 2008].

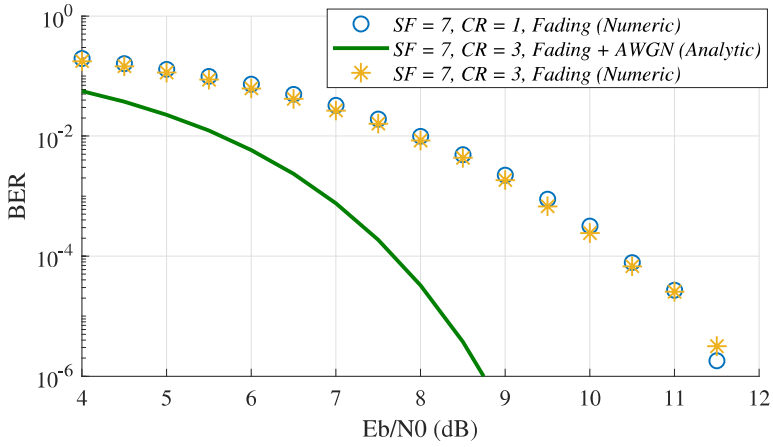

Figure 11 – BER *versus* E_b/N_0 for coded systems with $CR = 1$ and 3 in frequency-selective channels.

4 LoRaWan Basic Concepts

The basic concepts of LoRaWan and LPWAN, straightly related to the modulation format and maintained by the LoRa Alliance, are described in this Chapter. Concepts like architecture, classes, scalability, energy efficiency, and security are briefly discussed. The basic specification associated with LoRaWan applications in Brazil is also provided.

4.1 The LoRaWan Architecture

A LoRaWan network is normally composed of four parts, like those shown in Figure 12. The first part contains the end-devices or end-nodes, the units normally placed in the field, equipped with sensors or actuators [Rayes e Salam 2018]. The second part is composed by the gateways or concentrators, that communicate with the end-devices in bi-directional ways, via a star network topology, and through LoRa wireless connections, as shown in Fig. 13.(a). If there are multiple gateways in the vicinity of the end-device, all gateways receive the transmitted signals and forward the data to the LoRaWan server. The network server is responsible for all the logic of LoRaWan. It also handles all redundant messages provided by multiple gateways, as well as security verification, performs adaptive rate control, and schedules the best gateway for downlink communication to an end-device.

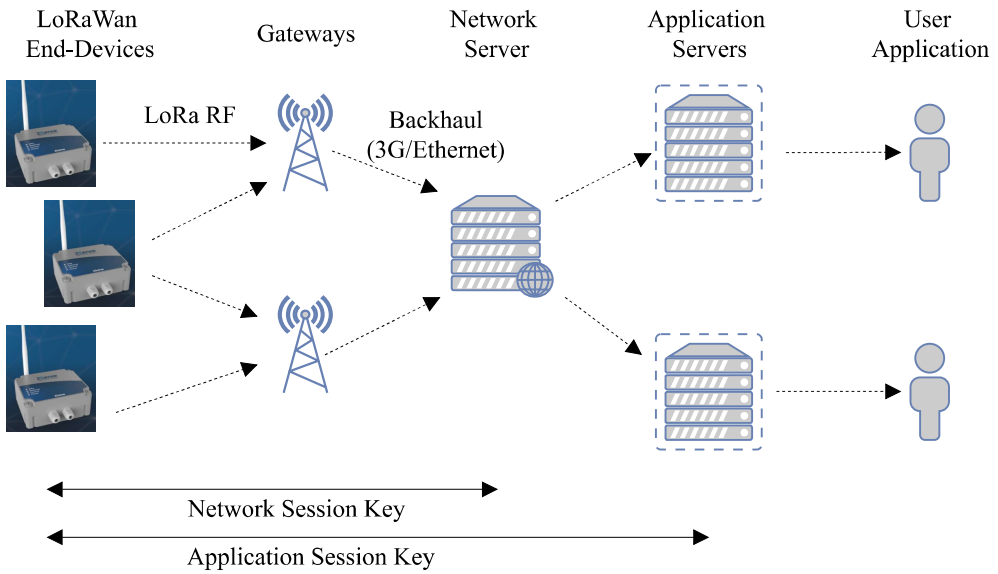

Figure 12 – LoRaWan end-to-end network architecture.

The final part is the application server, where users analyze the data sent by the end-devices. Normally, gateways communicate with the network server via a backhaul usually based on transmission control or user datagram protocols.

The LoRa Alliance chosen a star architecture for LoRaWan networks, mainly because, in such architecture, the end-devices can go into deep-sleep, thus drastically reducing the amount of consumed energy [SX1272/73 - 860 MHz to 1020 MHz Low Power Long Range Transceiver 2015]. Nevertheless, a mesh architecture can be adopted, as shown in Figure 13.(b). It can be verified, comparing the architectures of the Figures 13.(a) and 13.(b), that the star architecture eliminates the communication between end-devices, which also spare their batteries.

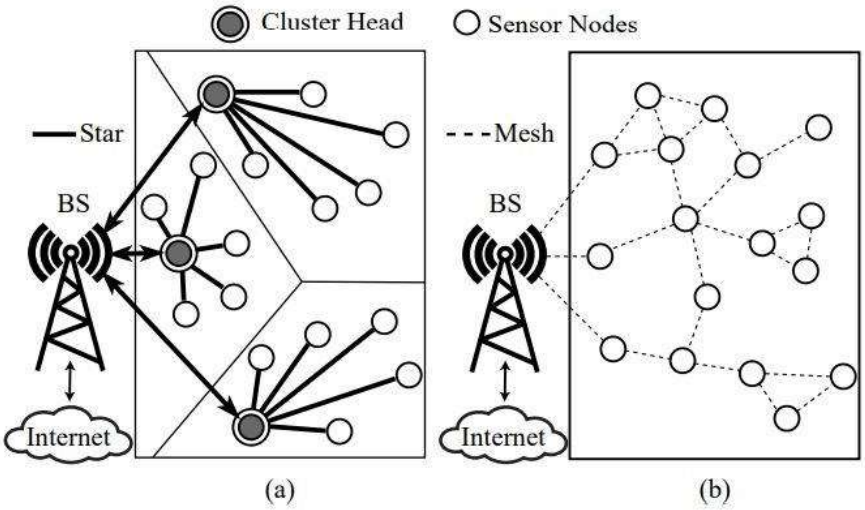

Figure 13 – (a) Star and (b) mesh architectures.

Even known that LoRa signals can be detected in a scenario with negative values of SNR, due to the modulation robustness against interference, obstacles that prevent line-of-sight still affecting the correct detection of LoRa data [Faber et al. 2020], [Staniec e Kowal 2018], [AN1200.22 LoRa™ Modulation Basics 2015]. In [dos Santos et al. 2019], a hybrid star and mesh LoRaWan was proposed to overcome problems with the absence of LOS, and where it is difficult to install more gateways, like in rural areas.

4.2 LoRaWan Classes and Energy Efficiency

Depending on the LoRaWan application, a trade-off between reliability and energy saving must be taken into account. Low power consumption should be considered in the applications running on batteries, which contrasts with the cases in which more reliable uplink and downlink transmissions are demanded. Because of this, LoRaWan provides three different types of classes, that mainly differentiate according to the manner the end-devices receive the data packets [Cheong et al. 2017]. Figure 14 shows that in class A, the network consumes the leased amount of energy, while still able to communicate in a bi-directional way, based on an ALOHA communication protocol.

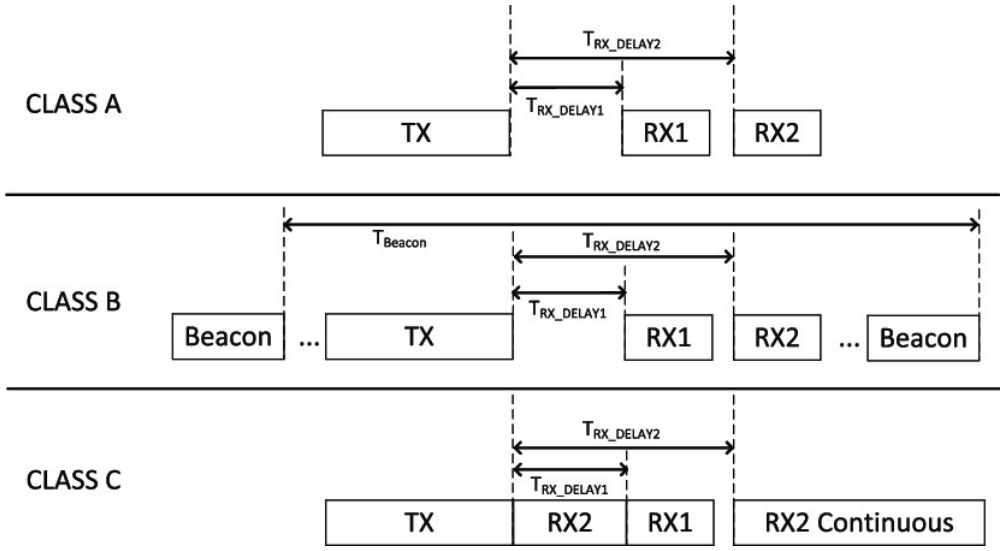

Figure 14 – LoRaWan classes.

In the ALOHA system, an end-device can, at any moment, wake-up and send uplink messages, without taking into consideration the possibility of collisions between transmissions. Immediately upon an uplink transmission at T_{rx_delay1}, the LoRaWan radio will open two reception windows RX1 and RX2. These are the two opportunities that the gateway has to send a downlink transmission to the end-device. If the gateway missed both of these receive windows, the end-device will go back to sleep. The gateway will only be able to send a downlink transmission after the next uplink.

Class B is pretty similar to class A, as it also has the bi-directional communication between end-device and gateway. However, while in class A the reception windows depend only on the uplink, in class B more windows are opened at scheduled intervals. For the gateway to send a downlink transmission, it needs to synchronize with the end-device, which occurs before in a time-synchronized beacon sent by the gateway. In class C, the end-devices maintains a continuous listening of downlink transmissions. The only moment they are not listening is when they are sending uplink messages. This results in low-latency between gateway and end-device. However, because the receiver is constantly listening (active) it uses much more energy than the end-devices in class A or B. This is why the use of this class is more appropriate in alternating current supplied applications.

4.3 Scalability and Security

Despite the robustness against interference and the ability to receive signals at SNR values as low as -20 dB, LoRaWan is affected by collisions from signals of other LoRaWan´s [Mahmood et al. 2018]. Because of this limitation, LoRaWan implements various techniques and regulations that allow scalability. LoRaWan gateways are able to receive signals with $SF = 7$ to 12, without aforetime knowing what SF the end-device is

using. Moreover, the gateways are able to listen up to 8 channels at the same time. The best receiver sensitivity is obtained by using $SF = 12$, but the time it takes to transmit a signal, also known as the time on-air (ToA) is also 32 times higher than the one provided with $SF = 7$ (see Chapter 2.3), which significantly increases the probability of a collision. For end-devices that have sufficiently stable RF conditions, a lower SF should be used. This can be done manually or by enabling adaptive data rate (ADR) procedures. If ADR is enabled, the gateways automatically adjust the data rate used in the communications with the end-devices.

Table 4 shows the data rates allowed in Brazil [LoRaWAN™ 1.1 Regional Parameters 2018]. The maximum ToA of transmission should not exceed 400 ms, which results in a maximum payload size for every DR, per transmission.

Table 4 – AU915-928 data rates.

Data Rate	**Configuration**	R_b **in b/s**	**Maximum payload (bytes)**
DR0	SF12/125kHz	250	59
DR1	SF11/125kHz	440	59
DR2	SF10/125kHz	980	59
DR3	SF9/125kHz	1760	123
DR4	SF8/125kHz	3125	230
DR5	SF7/125kHz	5470	230
DR6	SF8/500kHz	12500	230
DR7	Reserved	–	–
DR8	SF12/500kHz	980	41
DR9	SF11/500kHz	1760	117
DR10	SF10/5005kHz	3900	230
DR11	SF9/500kHz	7000	230
DR12	SF8/500kHz	12500	230
DR13	SF7/500kHz	21900	230
DR14 and DR15	Reserved	–	–

LoRaWan uses the two-layer AES-128 encryption and, when a packet is sent, it first gets encrypted with the application session key (AppSKey) and after with the network session key (NwkSKey). Fig. 12 shows that a packet is fully encrypted until it gets to the network server, where the packet is decrypted with the NwkSKey. This protects the data in a case where a rogue entity is able to intercept the LoRaWan packet in the RF part, or during transmission via a backbone technique to the network server. The LoRaWan packet will be forwarded to the application server, where it will be decrypted by the AppSKey. This protects the data if the network server is compromised.

LoRaWan support activation by personalization (ABP) and over-the-air activation (OTAA) methods to join an end-device to the network [Han e Wang 2018]. ABP is a static form of activation, in which the end-device needs to know beforehand the NwkSKey and AppSkey, as well as the device address (DevAddr). The simplicity of this form of activation is contrasted to its less security and scalability because the NwkSKey and AppSKey never change, and this could give a rogue entity more time to use brute force attacks. The OTAA method dynamically negotiates the NwkSKey and AppSKey with the network and application servers. In this case, the end-device doesn't need to know beforehand the NwkSKey and AppSKey. Instead, it needs to know the devices extended unique identifier (DevEUI), the application extended unique identifier (AppEUI), and the application key (AppKey). When an end-device wants to join a network, it will send a join request that includes the DevEUI and the AppEUI. This join request is then encrypted by the AppKey as shown in Fig. 15. When a join request is accepted, the application server generates an AppSKey and the network server creates a NwkSKey. Both will be returned through a downlink packet to the end-device. From that point, the end-device use the NwkSKey and the AppSKey in the same way as in ABP.

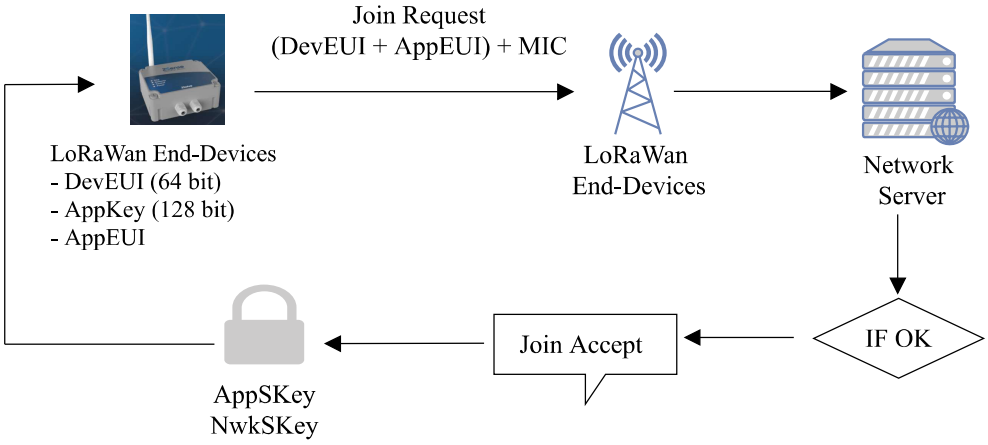

Figure 15 – LoRaWan OTAA join sequence.

Because the LoRaWan packet in both ABP and OTAA is encrypted, it is not possible to read the data by a rogue entity without the NwkSKey and AppSKey. Tampering is prevented by message integrity code (MIC), which is calculated and send in every transmitted packet. However, a replay attack is not prevented by the encryption and the MIC. To this aim, LoRaWan includes a frame counter (FC) in every packet. This 32-bit value reserved in both uplink (FCntUp) and downlink (FCntDown) is incremented at every transmission or data reception.

4.4 Basic Specifications for LoRaWan Ratification in Brazil

The Brazilian agency Anatel (*Agencia Nacional de Telecomunicações*) collaborated with equipment manufacturers and held public hearings prior the approval of the resolutions 14448 and 705 that regulate the LoRa technology in Brazil, defining the frequency plan for Latin America being the Australian standard of 923MHz (915MHz to 928MHz) [Resolução nº 705, de 21 de dezembro de 2018], [Ato nº 14448, de 04 de dezembro de 2017]. Table 5 shows the frequency plan used for LoRaWan by *the Things Network* network server in Brazil [The Things Network, LoRaWan frequency plans].

Table 5 – LoRaWan frequency plan in Brazil.

	Frequency MHz	**Value**
Uplink	916.8	SF7BW125; ...; SF10BW125
	917.0	SF7BW125; ...; SF10BW125
	917.2	SF7BW125; ...; SF10BW125
	917.4	SF7BW125; ...; SF10BW125
	917.6	SF7BW125; ...; SF10BW125
	917.8	SF7BW125; ...; SF10BW125
	918.0	SF7BW125; ...; SF10BW125
	918.2	SF7BW125; ...; SF10BW125
	917.5	SF8BW500
Downlink	923.3	SF7BW500; ...; SF12BW500
	923.9	SF7BW500; ...; SF12BW500
	924.5	SF7BW500; ...; SF12BW500
	925.1	SF7BW500; ...; SF12BW500
	925.7	SF7BW500; ...; SF12BW500
	926.3	SF7BW500; ...; SF12BW500
	926.9	SF7BW500; ...; SF12BW500
	927.5	SF7BW500; ...; SF12BW500

In Brazil, there are a couple of initiatives and companies that introduce LoRa and LoRaWan in Brazil. *The Things Network* TTN is LoRaWan server from the Netherlands, that is free to use. Their goal is to spread a free LoRaWan network all over the world, which is maintained by its community. TTN has the biggest LoRaWan community over the world, including a Brazilian branch [The Things Network - Brazil]. Their forum is a big source of information that includes the end-device modules, gateways, tutorial, regulation, among others.

AmericanTower is a commercial company, that has physical radio towers all over Brazil. They mainly rent tower space to big telecommunications companies, like *vivo*. In the last year, they stared in combination with local telecommunications companies, to roll out a LoRaWan network in Brazil, including Espirito Santo. Grande Vitoria should already have complete coverage [American Tower LoRaWan]. *Radioenge* is a company from Curitiba that designs LoRaWan and LoRaMesh modules that have an Anatel certification [RadioEnge].

4.5 The Expertise Developed at 2Solve Engenharia e Tecnologia

2Solve is an engineering solutions company located in Vitoria-ES, Brazil, mainly focused, but not limited to, in the oil and gas industry. Its activities can be separated into two fields: the first is related to dry-calibrate for on and offshore gas flow meters and the second focuses on designing customized engineering solutions. 2Solve is also highly active in Academics technology developments, keeping a close relationship with the Federal University of Espirito Santo. As a co-owner of 2Solve, the author of this thesis also used its knowledge of LoRa, obtained from this study, to design multiple IIoT devices that include LoRaWan. With a special notice to the *2STools 2Sense* and the *2STools Industrial Computer* devices, the following Subsections describe the basic functionalities of these devices. Commercial folders can be found in Appendix A and C.

4.5.1 The 2STools 2Sense End-Device

The 2STools 2Sense is a multi-function end-device capable of operating as a data-logger, basic control module, wireless gateway, and I/O repeater. Fig. 29 shows a folder of this device developed at 2Solve Engenharia e Tecnologia. This end-device is part of a product family automation system designed for IoT/Industry 4.0 that was created to facilitate the automation of small and large industrial processes. This makes the 2STools 2Sense a universal solution independent of the market segment.

Figure 16 – 2Sense: A final IoT solution. See Appendix A for further details.

In customized demands, it is possible to integrate additional sensing modules that are directly controlled by a SamD21 (an ARM-M0 micro-controller) through communication protocols like SPI and UART. The 2STools 2Sense has multiple sensor inputs (like pulse and frequency inputs), Modbus RTU over RS485 or RS232, a load cell input and four configurable 24-bit analog input configurable between 4 to 20 mA (or 0 to 10 V). It also has inputs for sensors type like PT100, PT1000 or thermocouple, and has the possibility to connect digital sensors via I^2C or One-Wire. The photo depicted in Fig. 30 shows that, beyond LoRa, several communication technologies can be adopted in different IIot applications.

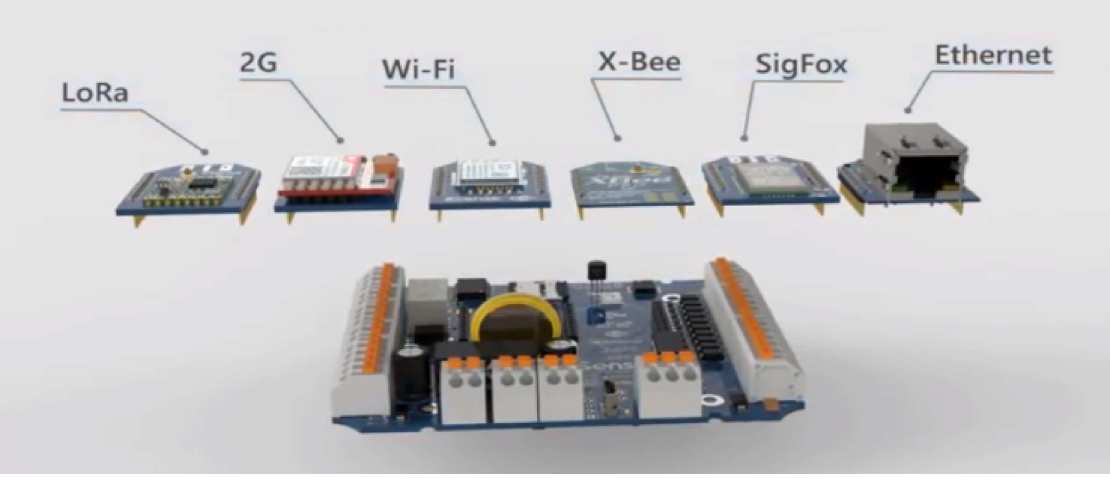

Figure 17 – Multiple communication modules implemented in the 2STools 2Sense device.

A realized use-case for the 2STools 2Sense, which included LoRaMesh, was the measurement of water level height in a mining dam drainage. Integrity is crucial in a mining dam because, if the excess water is obstructed, the water level in the drainage will rise and maintenance needs to be performed. By lowering a pressure sensor to the bottom of the drainage, it is possible to measure the amount of water present in that drainage. The pressure value can be read by the 2STools 2Sense and then, via LoRa, transmitted to a gateway.

4.5.2 The 2STools Industrial Computer

2STools Industrial Computer (2SToolsIC) is a hybrid automation solution that combines an industrial computer and a programmable logic controller functionality, based on an ARM Linux operating system. Using the 2SToolsIC, it is possible to acquire data, images, and control processes also from other equipment. This device is part of a family of automation products designed for IoT in Industry 4.0 designed to make automation of industrial processes easier and cheaper. This makes the 2SToolsIC, depicted in Fig. 31, a universal solution independent of the market segment. 2SToolsIC can operate over Wi-Fi or Ethernet and can also be configured as a Wi-Fi access point. Hence, it is possible to access

settings, to control equipment, to view process or diagnostic variables, and even to create a local network enabling access by mobile devices for voice and video communication.

Figure 18 – 2SToolsIC: An industrial computer. See Appendix C for further details.

An extension slot on the communication board of the 2SToolsIC is another great advantage because it offers a flexible way of adding other communication protocols. The modular feature of the board allows the addition of functions such as 3G, 4G and GPS, and also includes narrowband IoT technologies such as LoRaWan, LoRaMesh, Sigfox, or even XBee. Therefore, it can easily create mesh networks, reducing the cost with communication infrastructures.

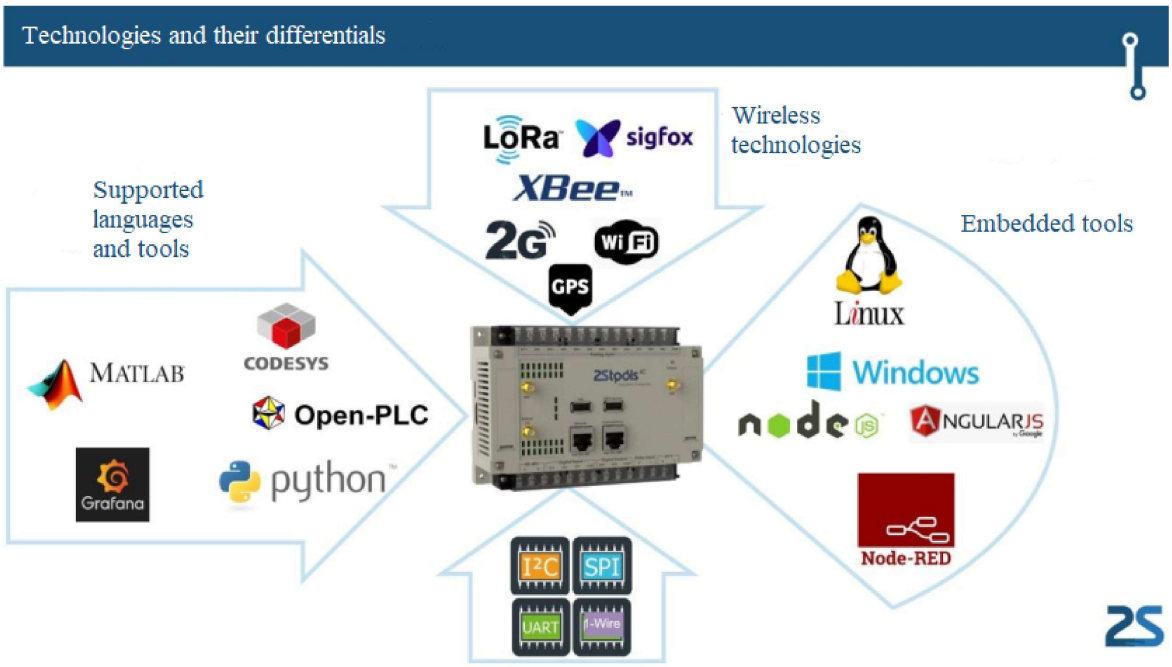

Figure 19 – The functionalities of the 2SToolsIC.

5 Experimental Evaluations of LoRaWan Systems

The experimental evaluations of LoRaWans in Urban, Suburban, and Open Areas, as well as in a Rural Area are reported in this Chapter. The experimental setups are described and the main results outlined emphasizing their approximations to the theoretical forecasts.

5.1 Evaluations in Urban, Suburban and Open Areas

An experimental setup with off-the-shelf LoRaWan equipment was prepared to demonstrate the feasibility of this promising technology, as well as the impact of the CR parameter on the packet error rate (PER), in a link with a single end-device.

5.1.1 The Experimental Setup

Fig. 20 shows a block diagram of the experimental setup used to measure RSSI, SNR, and N_oF. A global positioning system (GPS) module located at the transmitter (end device) measures the current device location, supported by an ATSAMD21 microcontroller with a clock of 48 MHz. The measured coordinates were periodically (every minute) transmitted, via an RFM95W LoRaWan chip, to the LoRa Gateway used as the receiver at a height of 154 m.

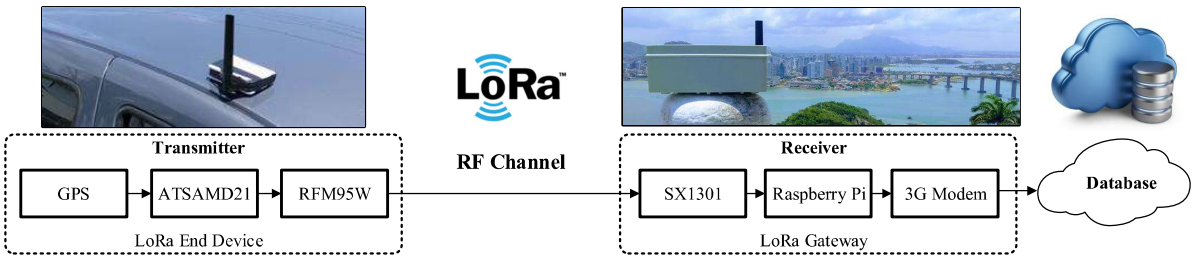

Figure 20 – Experimental setup with photos of the used LoRaWan devices.

At the receiver, the LoRa concentrator chip SX1301 measures a large amount of RSSI, SNR, and N_oF values at each end-device position. A Raspberry Pi microcomputer sends the measured values to a database via a 3G modem located at the LoRa Gateway. The used LoRa devices were configured according to the parameters shown in Table 6. These parameters were chosen based on a default configuration of a commonly used end-device, optimized for maximum link distances. In this configuration, SF is incremented at each transmission until looped around. The values of f_c represent the 8 channel frequencies

normally used in common LoRaWan gateways. The LoRaWan Gateway configuration can be found in Appendix D.

Table 6 – Parameters used in the evaluations in Urban, Suburban and Open areas.

Parameter	Symbol	Value	Unit
Bandwidth	B_W	125	kHz
Spreading Factor	SF	7; 8; 9; 10	-
Code Rate	CR	1	-
Frequency	f_c	902.3; 902.5; ...; 903.7	MHz
Transmission Power	-	20	dBm
Antennas Gain	-	3	dBi
Noise Figure	NF	7	dB

Fig. 21 shows the seven areas selected for the experiments. It can be seen from the map that, one is characterized as an urban area (UA#1), two defined as suburban areas (SA#1 and SA#2), and the remaining as open areas (OA#1 to OA#4). It should be noticed that, despite the existence of a lot of high buildings, a line-of-sight (LOS) was achieved in the SA#1 due to the existence of a straight avenue between the LoRa devices. It should be stressed that every dot depicted in Fig. 21 represents one transmission, which means that each one represents one measurement of RSSI and SNR.

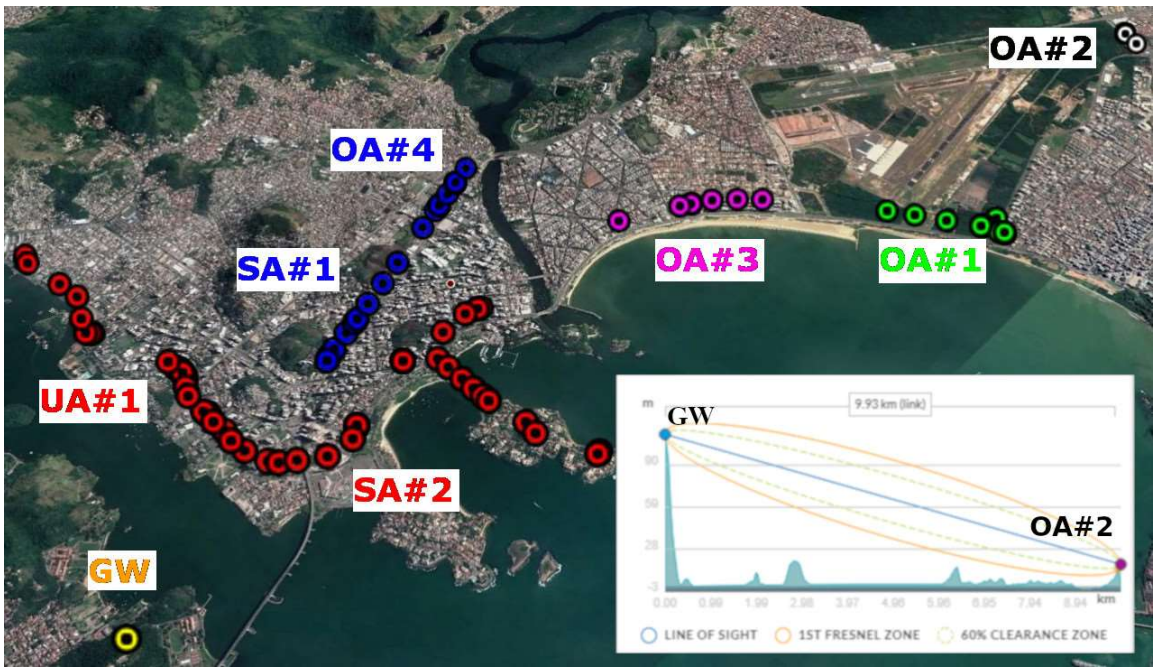

Figure 21 – Map of the areas selected for the measurements. UA: urban area, SA: suburban area; OA: open area. A Fresnel zone simulation is shown inset.

5.1.2 Experimental Results

Fig. 22 shows the RSSI values measured in all selected areas. To compare the measurements with analytic approximations, Fig. 22 shows curves of the Eqs. (12), (15) and (16). The gateway sensitivities for $SF = 7$ and 12 are also shown for fair comparisons. It can be seen from Fig. 22 that the above-mentioned areas can be distinguished from the RSSI measurements. However, some peculiarities entailed uncertainties in the classifications. Most of the measurements obtained at distances between 1 and ≈ 3.8 km belong to suburban areas, as indicated by comparison with the Hata model mathematically expressed in Eq. (15). Nevertheless, some RSSI values approach the magnitudes of urban (UA#1) and open areas. This can be explained by the mountain and the high buildings that exist in UA#1 and by the LOS that prevails between the gateway the itinerant end-device.

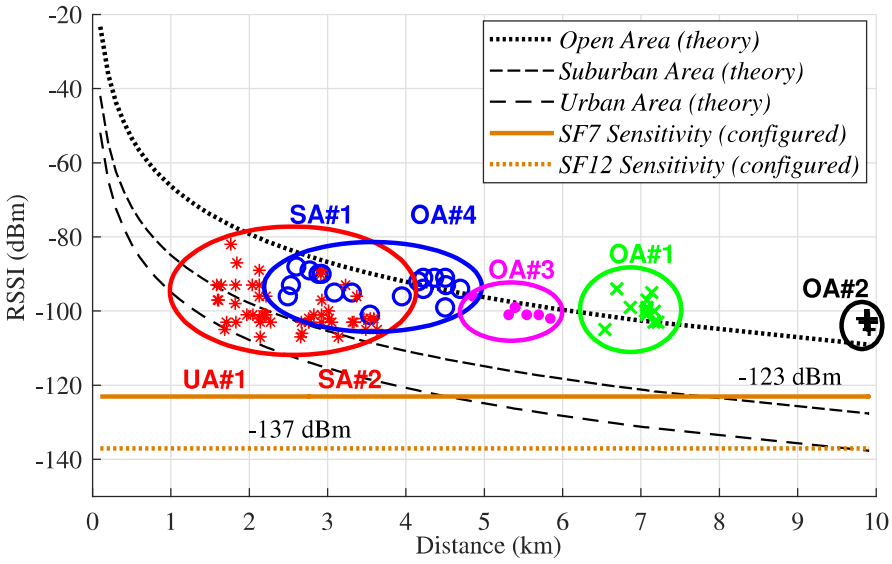

Figure 22 – Measurements of RSSIs at different distances (areas).

Similar behavior occurred in the measurements performed in SA#1 and OA#4 at distances between ≈ 2.8 and ≈ 5 km. At first glance, all those measurements should belong to a suburban area due to the number of buildings that exist in the region. However, the predominated LOS imposes an open area classification, as indicated by comparison with the Hata model of Eq. (16). It is worth noting the agreement between the theoretical path loss and the experimental RSSI measurements in OA#3. This was expected also due to the LOS, despite the transmission distance.

It should be stressed that some measurements obtained in OA#1 and all the RSSI values of OA#2 are slightly different from the Hata model due to the allocation of the end-device in locations with high relief when compared to the ground plane of SA#1. We conjecture that in those measurements no objects obstructed the Fresnel zone, as shown in inset Fig. 21. It can be seen from this inset that, unlike certain locations between SA#1 and SA#2 where the Fresnel zone is blocked, in the OA#2 it is not, also because of the

fact that the end-device was located around 20 m above the ground level of SA#1 area. The sensitivities for $SF = 7$ and 12, provided by the datasheet of the device are depicted in Fig. 22 to compare with the path losses provided by the above described Hata models, for the different considered distances [AN1200.22 LoRa™ Modulation Basics 2015]. It can be observed from Fig. 22 that the SF should be increased for transmission distance greater than ≈ 4.5 km in urban areas and 8 km in suburban areas. For the used LoRa devices, a 10 km communication in urban areas can be achieved only for a $SF = 12$.

Moreover, we compared the analytic noise floor generated by the Eq. (17) with an equivalent average value of NoF calculated from the measurements of RSSI and SNR. The average values of RSSI and SNR depicted in Figs 23.(a) and (b), respectively, were used to calculate the measured average noise floor shown in Fig. 23.(c). It should be note that the bandwidth used in the determination of NoF in equation (17) is the measurement bandwidth $B_W = 2 \cdot (8 \times 125) \approx 2000$ kHz (see the Frequency parameter of Table 7) that includes the 8 channels used by the gateway to capture the LoRa signals [SX1257 Low Power Digital I and Q RF Multi-PHY Mode Transceiver 2018]. Fig. 23.(c) shows the aforementioned comparison on the NoF parameter. The agreement between the theoretical NoF obtained from equation (17) and the average noise floor calculated from the measurements, shows the feasibility of the experimental evaluation.

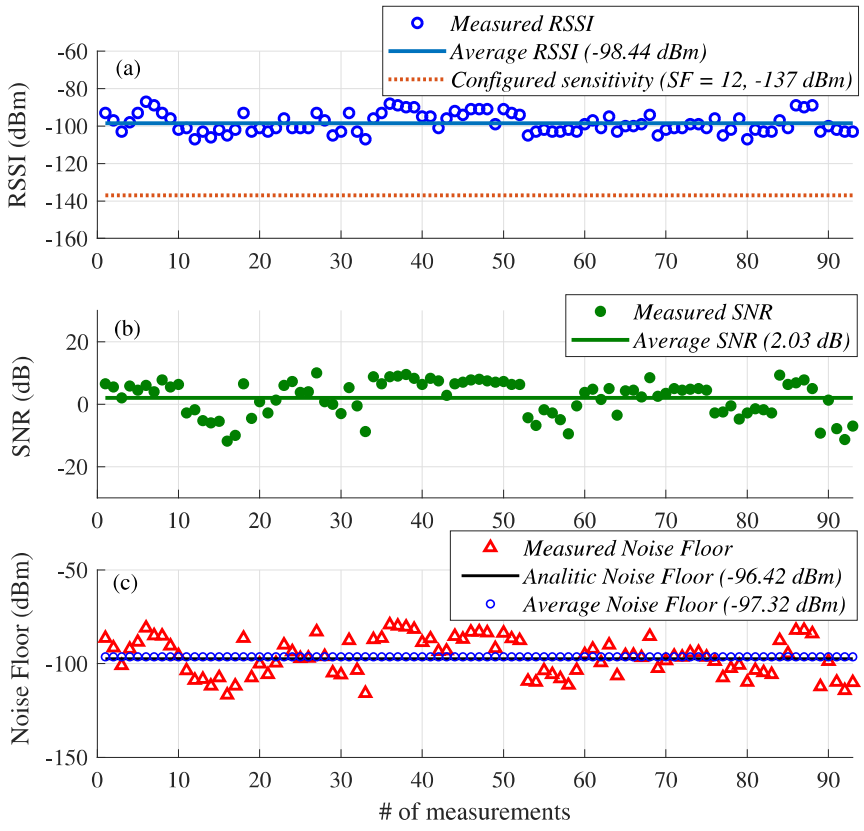

Figure 23 – (a) RSSI measurements. (b) The correspondent measured values of SNR. (c) Comparison of measured and analytic noise floor.

The impact of the code rates in the packet error rate is also important in the performance analysis of LoRaWan. Thus, considering the achievements of the above-described experiments and, in order to support the design of such LPWAN systems, we performed PER measurements considering transmission powers that allow packet losses, according to the received values of RSSI. Fig. 24 shows the measured values of PER for the specific transmitted powers, considering Hamming codes at rates $CR = 1$ and $CR = 3$. The code rates $CR = 2$ and $CR = 4$ were not contemplated because, in these situations, the systems only detect one error as is in the case of $CR = 1$ and $CR = 3$, respectively [Wells 1998].

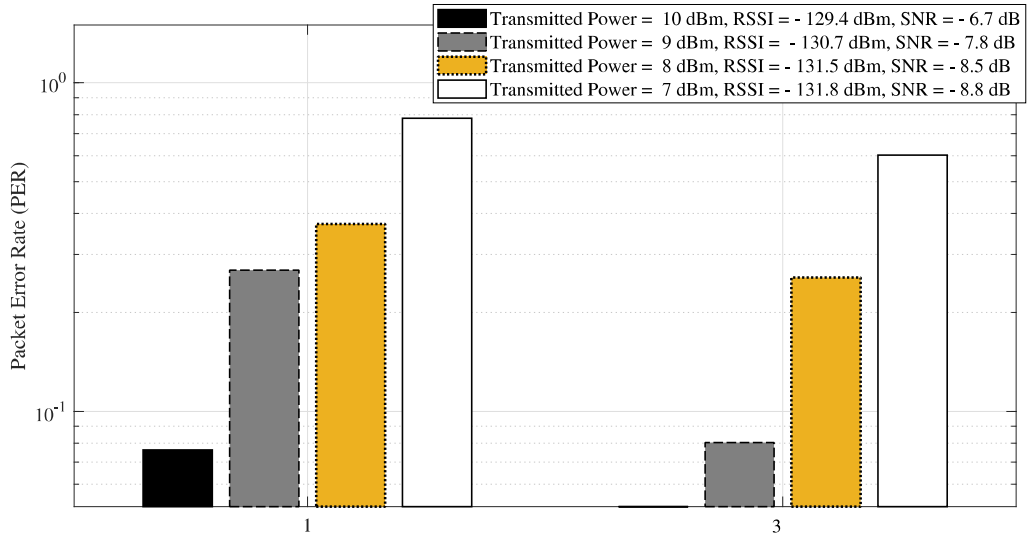

Figure 24 – Measurements of PER at $CR = 1$ and 3 obtained in a single gateway and a single end-device system, with $SF = 7$ and 3000 transmitted packets.

It can be observed from Fig. 24 that, unlike the behavior perceived in Fig. 10, the PER decreases with increments in the CR. We conjecture that this can be explained by the fact that, error correction can conduct to packet recovery, at the same time it increases the BER due to the modification in the useful bit rate and, in consequence, in the E_b/N_0, as described in Chapter 2.4. Nevertheless, the evaluations attest that the usage of FEC is extremely important in LoRaWan, specifically at distances and in areas where the values of RSSI are close to the receiver sensitivities.

The LoRa scalability, challenged in [Nolan, Guibene e Kelly 2016] and [Mahmood et al. 2018] to undertake the growth of end-devices connected to IoT, raised at this point. In accordance with the results presented in Fig. 25, a performance enhancement stated by the use of high values of CR, employed to overcome the interference provided by transmissions over the same spreading factors, as well as different SFs (that generally impacts scalability), can be presumed [Croce et al. 2018].

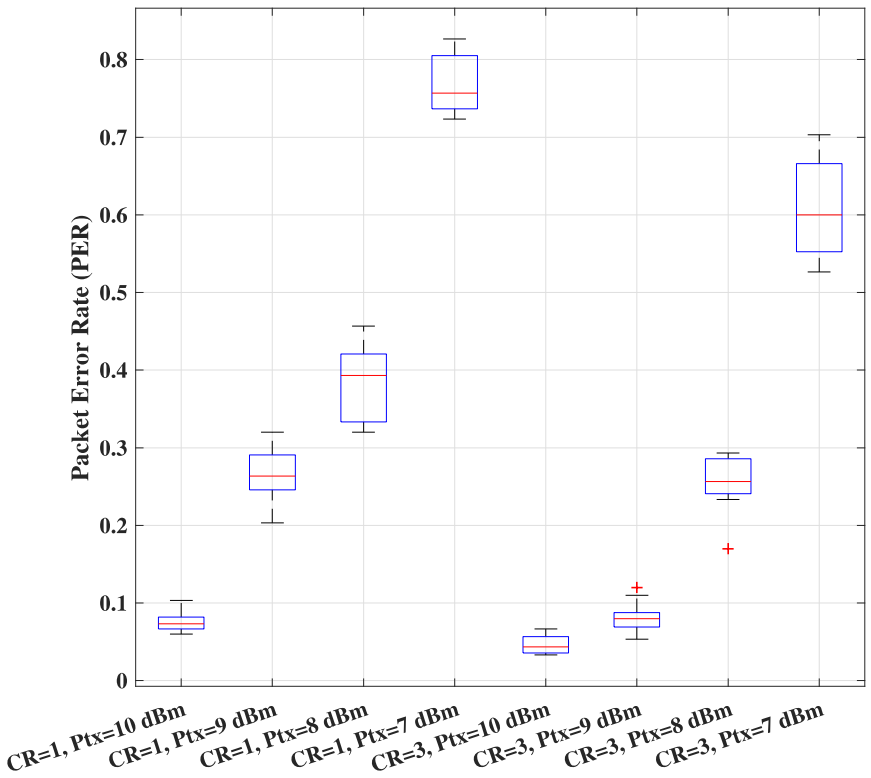

Figure 25 – Measurements of PER at $CR = 1$ and 3 obtained in a single gateway and a single end-device system, with $SF = 7$ and 3000 transmitted packets.

With these results, it is possible to conclude that communication in Urban and Open areas with distances up to ≈ 3 and ≈ 10 km, respectively, were successfully achieved according to measurements of the average received signal indicators around 100 dBm with an average SNR ≈ 5 dB. The usefulness of the practical analysis was confirmed by the agreement between the theoretical and the measured noise floors and by the verification of the impact of the code rate parameter on the systems packet error rate.

5.2 Evaluations in a Rural Area

A performance evaluation of the LoRaWan technology was also performed, to assess its feasibility in on-shore oil and gas industries [Faber et al. 2019].

5.2.1 The Experimental Setup

Fig. 26 shows the oil Industry map with the locations of the central monitoring station (Gateway location) and several oil wells (end devices locations). It should be noticed that the devices and the general configurations employed in the Urban areas evaluations were used in this analysis. The LoRaWan devices were configured according to the parameters shown in Table 7.

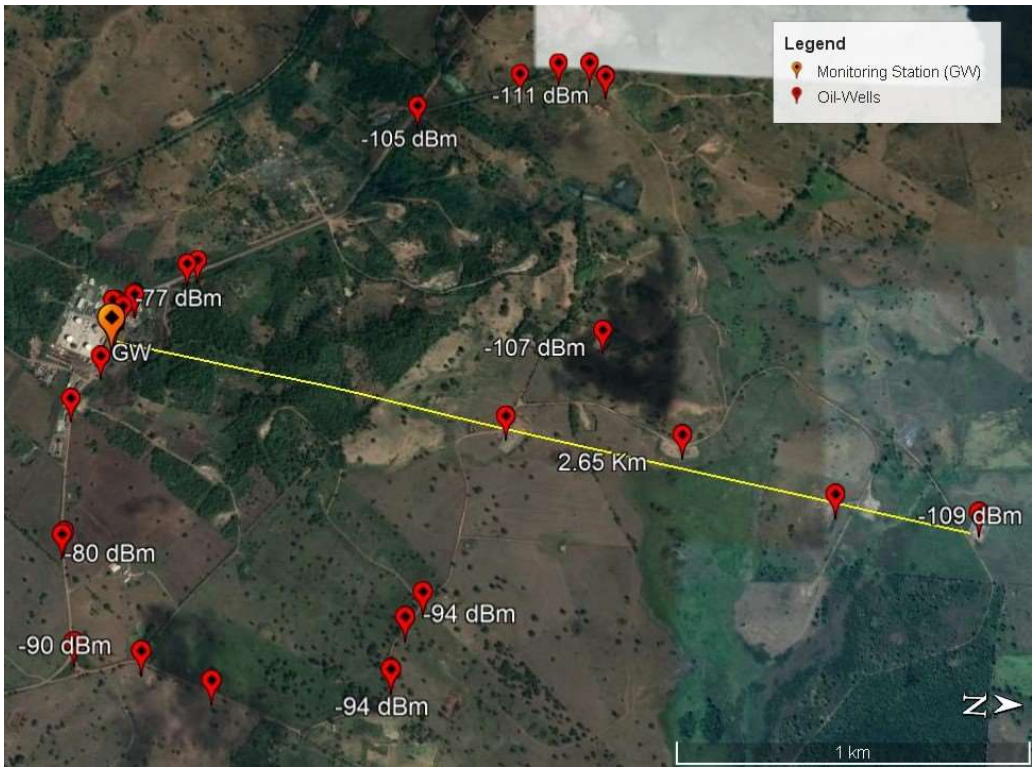

Figure 26 – Map showing the central monitoring station and the oil wells.

Table 7 – Parameters configured in the devices for Rural Area.

Parameter	Symbol	Value	Unit
Bandwidth	B_W	125	kHz
Spreading Factor	SF	10	-
Frequency	f_c	902.3; 902.5; ...; 903.7	MHz
Transmission Power	-	20	dBm
Noise Figure	NF	7	dB
Antennas Gain	-	3	dBi
Gateway Antenna Height	-	20	m
End-Device Antenna Height	-	1.5	m

5.2.2 Experimental Results

Fig. 27 shows the RSSI values measured in all considered oil wells. To compare the measurements with analytic approximations, Fig. 27 shows the curve of Eq. (16). The gateway sensitivities for $SF = 10$ is also shown for fair comparisons. It is clear from Fig. 27 that the behavior of open areas can be distinguished from the RSSI measurements. This was expected due to the fact that the monitoring plant is located in a rural area. The few measurements that belong to suburban areas can be explained by the mountains and high trees that exist between the monitoring station and the oil wells. Fig. 27 also shows that, for all measurements, the acquired RSSI values are above the receiver sensitivity. This shows the robustness of the technology in such a scenario.

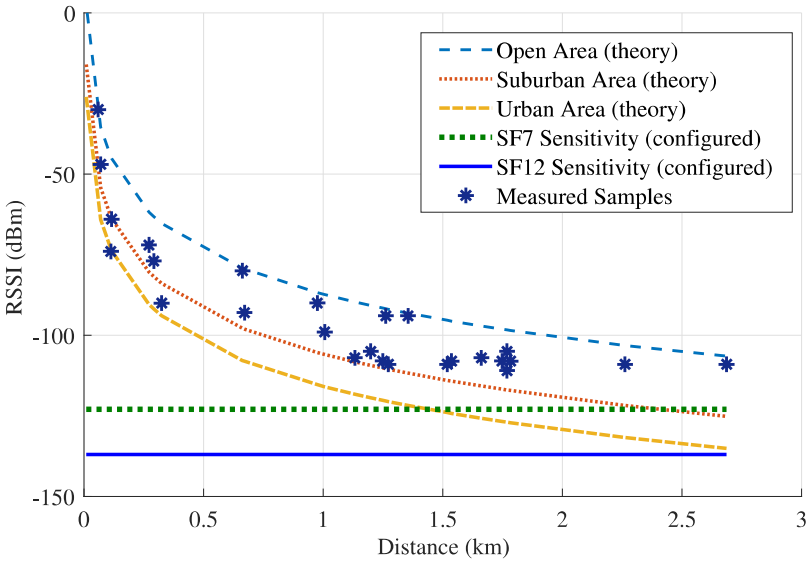

Figure 27 – Measurements of RSSIs at different oil wells.

Fig. 28 shows a comparison between the measured values of SNR and the SNR quantities estimated from the measured RSSIs. It can be seen from Fig. 27 that, almost all the estimated values are close to measured SNRs. The discrepancy registered in the first measurements is due to the fact that they were measured underneath the gateway antenna tower, whereas the last three depicted discrepancies can be explained by multipath gains not considered by the theoretical analysis. Nevertheless, it is possible to conclude that communication between a central oil-producing process used to monitor several oil wells, located in a rural area, was successfully achieved at distances up to ≈ 2.7 km, according to measurements of average received signal indicators around 100 dBm with an average SNR around 5.6 dB.

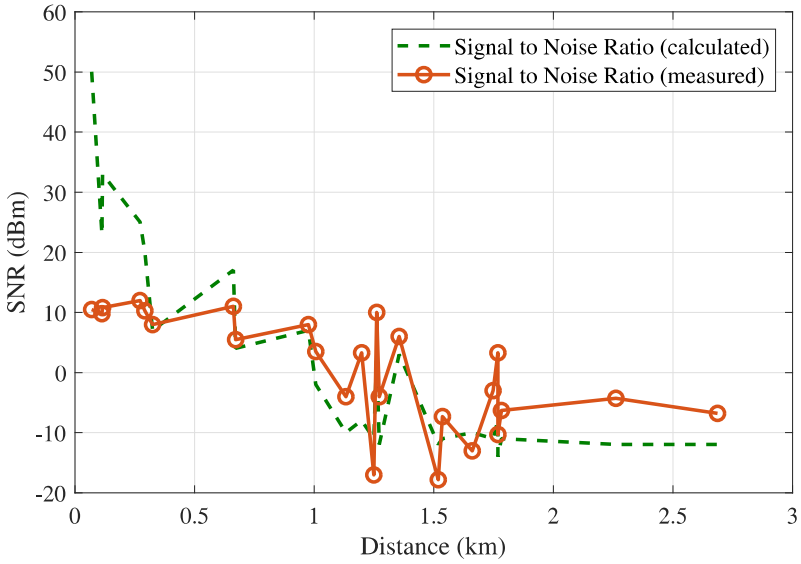

Figure 28 – Measured and estimated (from RSSI) values of SNR.

6 Conclusion and Future Works

Important mechanisms of the LoRa physical layer that can support the design of a LoRaWan are still unknown due to its corporate property nature. Believing that a better understanding of their functionalities can assist the combat of technology challenges like reliability, we presented a theoretical and experimental evaluation of LoRaWan links with a single end-device for both an urban and rural areas.

We assessed the LoRa performance in additive white Gaussian noise channels through a numerical model, to elucidate its communication capabilities in negative signal-to-noise ratio conditions. We also proposed an analytic bit-error-rate expression to analyze the influence of the LoRa code rate parameter in the overall system performance. The agreement between the theoretical and the numerical results of a Hamming coded LoRa system validated the closed-form BER in AWGN channels, highlighting the significance of forward error correction codes in the LoRa PHY model.

An experimental setup was prepared to demonstrate the feasibility of LoRaWan in the long-range coverage, as well as the impact of the code rate parameter on the system packet error rate. Communication in urban and open areas with distances up to ≈ 3 and ≈ 10 km, respectively, were achieved, according to measurements of the average received signal indicators around -100 dBm for an average SNR ≈ 5 dB. The agreement between the theoretical and the measured noise floors, and the confirmation of the significant impact of the parameter CR on the system PER, show the usefulness of the experimental analysis in future designs/deployments of such LPWAN systems.

In the rural areas evaluations, communication in distances up to ≈ 2.7 km was achieved, according to measurements of the average received signal indicators around -100 dBm for an average SNR ≈ 5.6 dB. Thus, we conclude that LoRaWan can be considered a suitable LPWAN technology for smart monitoring in gas and oil Industries.

The impact of different code rates, as well as different codification schemes, in LoRaWan´s with multiple gateways and end-devices, should be evaluated in our future works, through optimization algorithms. The integration of parameter optimizations with virtualization and cloud computing processes can also be adopted in future setups, aiming performance enhancements.

References

AL-FUQAHA, A. et al. Internet of things: A survey on enabling technologies, protocols, and applications. *IEEE Communications Surveys & Tutorials*, IEEE, v. 17, n. 4, p. 2347–2376, 2015. Cited 2 times on pages 1 and 2

ALL About LoRa and LoRaWAN. <https://www.sghoslya.com/>. Accessed: 2018-10-20. Cited on page 15

AMERICAN Tower LoRaWan. <http://www.americantower.com.br/pt/solutions/atc-lorawan-network/cidades-onde-estamos-presentes/index.htm>. Accessed: 2020-06-13. Cited on page 31

AN1200.13 SX1272/3/6/7/8: LoRa Modem. 1. ed. [S.l.], 2013. Cited 4 times on pages 9, 13, 14, and 17

AN1200.22 LoRa™ Modulation Basics. 2. ed. [S.l.], 2015. Cited 9 times on pages 2, 9, 10, 11, 13, 14, 21, 26, and 38

ANGRISANI, L. et al. Lora protocol performance assessment in critical noise conditions. In: IEEE. *2017 IEEE 3rd International Forum on Research and Technologies for Society and Industry (RTSI)*. [S.l.], 2017. p. 1–5. Cited on page 6

ATO nº 14448, de 04 de dezembro de 2017. <https://www.anatel.gov.br/legislacao/en/atos-de-requisitos-tecnicos-de-certificacao/2017/1139-ato-14448>. Accessed: 2020-05-04. Cited on page 30

AUGUSTIN, A. et al. A study of lora: Long range & low power networks for the internet of things. *Sensors*, Multidisciplinary Digital Publishing Institute, v. 16, n. 9, p. 1466, 2016. Cited on page 13

CAPUZZO, M.; MAGRIN, D.; ZANELLA, A. Confirmed traffic in lorawan: Pitfalls and countermeasures. In: IEEE. *2018 17th Annual Mediterranean Ad Hoc Networking Workshop (Med-Hoc-Net)*. [S.l.], 2018. p. 1–7. Cited on page 7

Chen, B. et al. Smart factory of industry 4.0: Key technologies, application case, and challenges. *IEEE Access*, v. 6, p. 6505–6519, 2018. ISSN 2169-3536. Cited on page 1

Cheong, P. S. et al. Comparison of lorawan classes and their power consumption. In: *2017 IEEE Symposium on Communications and Vehicular Technology (SCVT)*. [S.l.: s.n.], 2017. p. 1–6. Cited on page 26

CHO, Y. S. et al. *MIMO-OFDM wireless communications with MATLAB*. [S.l.]: John Wiley & Sons, 2010. Cited on page 24

CROCE, D. et al. Impact of lora imperfect orthogonality: Analysis of link-level performance. *IEEE Communications Letters*, IEEE, v. 22, n. 4, p. 796–799, 2018. Cited on page 39

dos Santos, W. G. V. et al. Sensor allocation in a hybrid star-mesh iot network using genetic algorithm and k-medoids. In: *2019 IEEE Latin-American Conference on Communications (LATINCOM)*. [S.l.: s.n.], 2019. p. 1–6. Cited on page 26

ELSHABRAWY, T.; ROBERT, J. Closed-form approximation of lora modulation ber performance. *IEEE Communications Letters*, IEEE, v. 22, n. 9, p. 1778–1781, 2018. Cited 3 times on pages 6, 10, and 13

ESTUDO IoT na AL 2019 – Inter-American Development Bank. 2019. Cited on page 2

FABER, M. et al. Performance evaluation of lorawan applied to smart monitoring in onshore oil industries. 2019. Cited on page 40

Faber, M. J. et al. A theoretical and experimental evaluation on the performance of lora technology. *IEEE Sensors Journal*, p. 1–1, 2020. Cited 2 times on pages 23 and 26

Farooq, M. O.; Pesch, D. Analyzing lora: A use case perspective. In: *2018 IEEE 4th World Forum on Internet of Things (WF-IoT)*. [S.l.: s.n.], 2018. p. 355–360. Cited on page 9

GEORGIOU, O.; RAZA, U. Low power wide area network analysis: Can lora scale? *IEEE Wireless Communications Letters*, IEEE, v. 6, n. 2, p. 162–165, 2017. Cited on page 10

HAN, J.; WANG, J. An enhanced key management scheme for lorawan. *Cryptography*, Multidisciplinary Digital Publishing Institute, v. 2, n. 4, p. 34, 2018. Cited on page 29

HOELLER, A. et al. Analysis and performance optimization of lora networks with time and antenna diversity. *IEEE Access*, IEEE, v. 6, p. 32820–32829, 2018. Cited on page 7

JUN, A. D. et al. Modeling and simulation of lora in opnet. In: *Advanced Multimedia and Ubiquitous Engineering*. [S.l.]: Springer, 2017. p. 551–559. Cited on page 13

Kuo, Y. et al. Design of a wireless sensor network-based iot platform for wide area and heterogeneous applications. *IEEE Sensors Journal*, v. 18, n. 12, p. 5187–5197, June 2018. ISSN 1530-437X. Cited on page 1

Lauridsen, M. et al. Coverage comparison of gprs, nb-iot, lora, and sigfox in a 7800 km^2 area. In: *2017 IEEE 85th Vehicular Technology Conference (VTC Spring)*. [S.l.: s.n.], 2017. p. 1–5. Cited on page 2

LORAWAN™ 1.1 Regional Parameters. B. [S.l.], 2018. Cited on page 28

LUVISOTTO, M. et al. On the use of lorawan for indoor industrial iot applications. *Wireless Communications and Mobile Computing*, Hindawi, v. 2018, 2018. Cited on page 7

MAHMOOD, A. et al. Scalability analysis of a lora network under imperfect orthogonality. *IEEE Transactions on Industrial Informatics*, IEEE, v. 15, n. 3, p. 1425–1436, 2018. Cited 2 times on pages 27 and 39

Navarro-Ortiz, J. et al. Integration of lorawan and 4g/5g for the industrial internet of things. *IEEE Communications Magazine*, v. 56, n. 2, p. 60–67, Feb 2018. ISSN 0163-6804. Cited on page 1

NOLAN, K. E.; GUIBENE, W.; KELLY, M. Y. An evaluation of low power wide area network technologies for the internet of things. In: IEEE. *Wireless Communications and Mobile Computing Conference (IWCMC), 2016 International*. [S.l.], 2016. p. 439–444. Cited on page 39

PARK, J. J.; CHEN, S.-C.; CHOO, K.-K. R. *Advanced Multimedia and Ubiquitous Engineering: MUE/FutureTech 2017*. 1. ed. [S.l.]: Cambridge University Press, 2017. ISBN 978-9811050404. Cited on page 13

PROAKIS, J.; SALEHI, M. Digital communications. McGraw-Hill, 2008. Disponível em: <https://books.google.com.br/books?id=ksh0GgAACAAJ>. Cited 3 times on pages 15, 22, and 24

Qadir, Q. M. et al. Low power wide area networks: A survey of enabling technologies, applications and interoperability needs. *IEEE Access*, v. 6, p. 77454–77473, 2018. ISSN 2169-3536. Cited 2 times on pages 1 and 2

RADIOENGE. <https://www.radioenge.com.br/>. Accessed: 2020-06-13. Cited on page 31

RAYES, A.; SALAM, S. *Internet of Things From Hype to Reality: The Road to Digitization*. Springer International Publishing, 2018. ISBN 9783319995168. Disponível em: <https://books.google.com.br/books?id=EqR5DwAAQBAJ>. Cited on page 25

Raza, U.; Kulkarni, P.; Sooriyabandara, M. Low power wide area networks: An overview. *IEEE Communications Surveys Tutorials*, v. 19, n. 2, p. 855–873, Secondquarter 2017. ISSN 1553-877X. Cited on page 2

RESOLUçãO nº 705, de 21 de dezembro de 2018. <https://www.anatel.gov.br/legislacao/resolucoes/2018/1220-resolucao-705>. Accessed: 2020-05-04. Cited on page 30

REYNDERS, B.; MEERT, W.; POLLIN, S. Range and coexistence analysis of long range unlicensed communication. In: *23rd International Conference on Telecommunications (ICT)*. [S.l.]: IEEE, 2016. Cited 2 times on pages 6 and 13

REYNDERS, B.; POLLIN, S. Chirp spread spectrum as a modulation technique for long range communication. In: IEEE. *Communications and Vehicular Technologies (SCVT), 2016 Symposium on*. [S.l.], 2016. p. 1–5. Cited 6 times on pages 2, 6, 9, 10, 13, and 18

SELLER, O. B.; SORNIN, N. *Low power long range transmitter*. [S.l.]: European Patent Application, 2014. EP 2763321A1. Cited 3 times on pages 10, 22, and 23

SØRENSEN, R. B. et al. Analysis of latency and mac-layer performance for class a lorawan. *arXiv preprint arXiv:1712.05171*, 2017. Cited on page 2

STANIEC, K.; KOWAL, M. Lora performance under variable interference and heavy-multipath conditions. *Wireless Communications and Mobile Computing*, Hindawi, v. 2018, 2018. Cited 6 times on pages 2, 9, 15, 17, 22, and 26

SX1257 Low Power Digital I and Q RF Multi-PHY Mode Transceiver. 1. ed. [S.l.], 2018. Cited on page 38

SX1272/73 - 860 MHz to 1020 MHz Low Power Long Range Transceiver. 3. ed. [S.l.], 2015. Cited 2 times on pages 10 and 26

SX1276/77/78/79 - 137 MHz to 1020 MHz Low Power Long Range Transceiver. 6. ed. [S.l.], 2019. Cited on page 10

THE Things Network - Brazil. <https://www.thethingsnetwork.org/country/brazil/>. Accessed: 2020-06-13. Cited on page 30

THE Things Network, LoRaWan frequency plans. <https://www.thethingsnetwork.org/docs/lorawan/frequency-plans.html>. Accessed: 2020-05-04. Cited on page 30

VANGELISTA, L. Frequency shift chirp modulation: The lora modulation. *IEEE Signal Processing Letters*, IEEE, v. 24, n. 12, p. 1818–1821, 2017. Cited 4 times on pages 6, 9, 10, and 17

Vejlgaard, B. et al. Interference impact on coverage and capacity for low power wide area iot networks. In: *2017 IEEE Wireless Communications and Networking Conference (WCNC)*. [S.l.: s.n.], 2017. p. 1–6. ISSN 1558-2612. Cited on page 2

WELLS, R. B. *Applied coding and information theory for engineers*. [S.l.]: Prentice-Hall, Inc., 1998. Cited 3 times on pages 11, 22, and 39

Wunder, G. et al. 5gnow: non-orthogonal, asynchronous waveforms for future mobile applications. *IEEE Communications Magazine*, v. 52, n. 2, p. 97–105, February 2014. ISSN 0163-6804. Cited on page 1

Xu, L. D.; He, W.; Li, S. Internet of things in industries: A survey. *IEEE Transactions on Industrial Informatics*, v. 10, n. 4, p. 2233–2243, Nov 2014. ISSN 1551-3203. Cited on page 1

Yang, B. et al. Digital beamforming-based massive mimo transceiver for 5g millimeter-wave communications. *IEEE Transactions on Microwave Theory and Techniques*, v. 66, n. 7, p. 3403–3418, July 2018. Cited on page 1

Yasmin, R. et al. On the integration of lorawan with the 5g test network. In: *2017 IEEE 28th Annual International Symposium on Personal, Indoor, and Mobile Radio Communications (PIMRC)*. [S.l.: s.n.], 2017. p. 1–6. ISSN 2166-9589. Cited on page 1

YIM, D. et al. An experimental lora performance evaluation in tree farm. In: IEEE. *2018 IEEE Sensors Applications Symposium (SAS)*. [S.l.], 2018. p. 1–6. Cited on page 7

Appendices

A The Expertise Developed at 2Solve Engenharia e Tecnologia

2Solve is an engineering solutions company located in Vitoria-ES, Brazil, mainly focused, but not limited to, in the oil and gas industry. Its activities can be separated into two fields: the first is related to dry-calibrate for on and offshore gas flow meters and the second focuses on designing customized engineering solutions. 2Solve is also highly active in Academic technology developments, keeping a close relationship with the Federal University of Espírito Santo. As a co-owner of 2Solve, the author of this thesis also used its knowledge of LoRa, obtained from this study, to design multiple IIoT devices that include LoRaWan.

A.1 The 2STools 2Sense End-Device

The 2STools 2Sense is a multi-function end-device capable of operating as a data-logger, as well as a basic control module, a wireless gateway, and an I/O repeater. Fig. 29 shows a folder of this device developed at 2Solve Engenharia e Tecnologia. This end-device is part of a product family automation system designed for IoT / Industry 4.0 that was created to facilitate the automation of small and large industrial processes. This makes the 2STools 2Sense an universal solution, independent of the market segment.

Figure 29 – A picture of the 2STools 2Sense end-device. See Appendix B for further details.

In customized demands, it is possible to integrate additional sensing modules that are directly controlled by the SamD21 (an ARM-M0 micro-controller) through communication protocols like SPI (Serial Peripheral Interface) and UART (Universal Asynchronous Receiver-Transmitter). The 2STools 2Sense has multiple sensor inputs,

including pulse and frequency inputs, Modbus RTU over RS485 or RS232, a load cell input, four configurable 24-bit analog input configurable between 4 to 20 mA or 0 to 10V. It also has inputs for sensors like PT100, PT1000 or thermocouple, and the possibility to connect digital sensors via I^2C or One-Wire. Fig. 30 shows that, beyond LoRa, several communication technologies can be adopted in different IIoT applications.

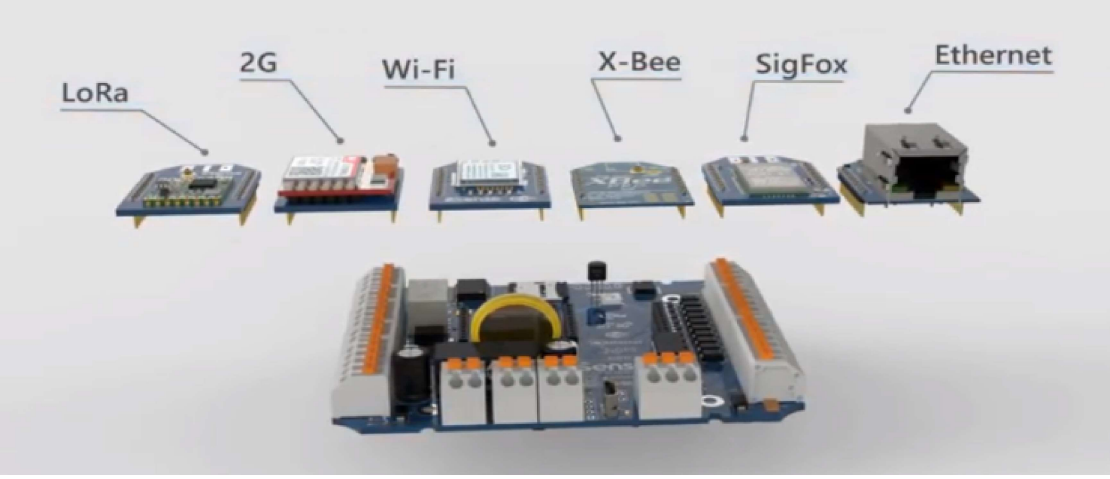

Figure 30 – Multiple communication modules implemented in the 2STools 2Sense device.

A realized use-case for the 2STools 2Sense, which included LoRaMesh, was the measurement of water level height in a mining dam drainage. Integrity is crucial in a mining dam because, if the excess water is obstructed, the water level in the drainage will rise and maintenance needs to be performed. By lowering a pressure sensor to the bottom of the drainage, it is possible to measure the amount of water present in the drainage. The pressure value can be measured by the 2STools 2Sense and then, via LoRa, transmitted to a gateway.

A.2 The 2STools Industrial Computer

2STools Industrial Computer (2SToolsIC) is a hybrid automation solution that combines an industrial computer and a programmable logic controller functionality, based on an ARM Linux operating system. Using the 2SToolsIC, it is possible to acquire data, images, and control processes from other equipment. This device is part of a family of automation products designed for IoT/Industry 4.0, to make automation of industrial processes easier and cheaper. This makes the 2SToolsIC depicted in Fig. 31 an universal solution, independent of the market segment. 2SToolsIC can operate over Wi-Fi or Ethernet, and can also be configured as a Wi-Fi access point. With this, it is possible to access settings, control equipment, view process or diagnostic variables, and even create a local network enabling access by mobile devices for voice and video communication.

Figure 31 – A picture of the the 2STool industrial computer. See Appendix C for further details.

An extension slot on the communication board of the 2SToolsIC is another great advantage, that offers a flexible way of adding other communication protocols. The modular feature of the board allows the addition of functions such as 3G/4G, GPS, and also includes narrowband IoT technologies such as LoRaWan, LoRaMesh, Sigfox, or even XBee to easily create mesh networks, reducing the cost with communication infrastructure.

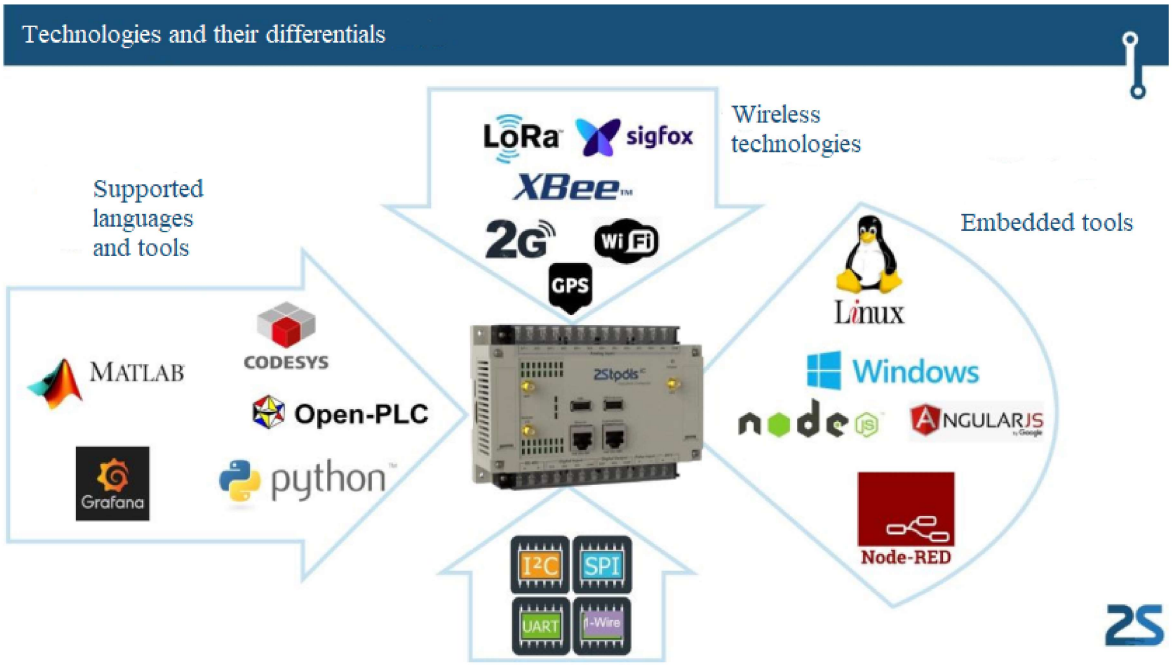

Figure 32 – The functionalities of the 2SToolsIC.

2Solve
ENGENHARIA E TECNOLOGIA

The 2Sense is a multifunction device capable of operating as a datalogger, basic control module, wireless gateway, and I/O repeater.

This device is part of a family of automation products designed for IoT / Industry 4.0 that were created to facilitate and cheapen the automation of small and large industrial processes. This makes **2Sense** a universal, industry-independent solution.

2Sense can be purchased with standard features and freely configuration by the user or it can have specific firmware running routines dedicated to a particular application. The development of specific firmware for a given application is a strategy of 2Solve to enable customization at a low cost.

Through the configuration tool or a customized configuration, it is possible to process acquired data and execute logics using physical inputs and outputs, variables and parameters mapped from another device.

This product was developed to guarantee flexibility for the most diverse applications. For this reason, 2Sense can be supplied with different combinations of inputs, outputs, and wired or wireless communication ports. This provides easy adaptation to any plant or equipment, regardless of size.

The **2Sense** natively has a slot for Micro SD cards up to 32GB, a digital input, a digital relay output, and an I^2C and 1-Wire bus. The busses enable the integration of display, digital sensors, magnetometer, accelerometer, gyroscope, and a wide range of sensors and actuators that are constantly being developed.

This feature increases the power of the 2Sense incredibly because using this concept, it is possible to integrate dozens of sensors in a single device. In addition to the advantage of a number of sensors, the concept makes possible the simultaneous integration in a single bus, sensors of different purposes, such as humidity, temperature, vibration, luminosity, sound, etc.

Av. Fernando Ferrari, 1080
Ed. América Centro Empresarial
Torre Central, sala 403
Mata da Praia, Vitória/ES
29066-380

B 2STools 2Sense Folder

2Solve
ENGENHARIA E TECNOLOGIA

In customized demands, it is possible to integrate additional sensing modules and control them directly with the microcontroller through the SPI and UART ports.

The 2Sense is supplied with a pulse input, RS485 RTU, input for load cell, 3 analog inputs, switchable between 4 to 20mA or 0 to 10V, an input for PT100, PT1000 or thermocouple.

The 2Sense has two slots for wired and wireless communication modules, in order to enable the integration of the device with networks and other master or slave devices.

Depending on the product configuration, it is possible to use two equal or different technologies in redundancy.

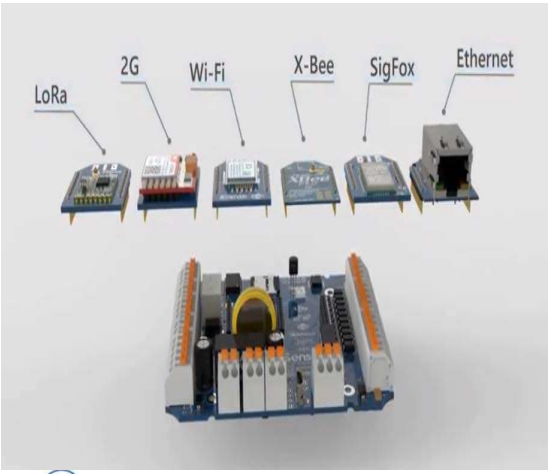

The modular characteristic feature allows adding functions such as WiFi, Bluetooth, Ethernet, GPRS, GPS, among other technologies and protocols, including **LPWAN** technologies such as LoRaWAN, LoRaMesh, and XBee, which can facilitate the formation of mesh networks with ease, greatly reducing the cost of communication infrastructure.

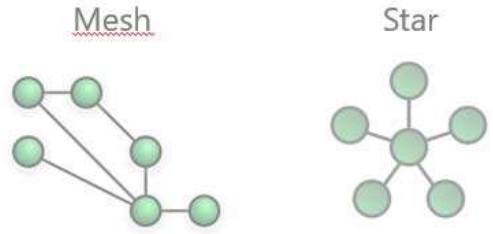

The 2Sense can be supplied with different wireless modules, like LoRaWAN, LoRaMesh, XBee, Sigfox, 3G/4G, etc.

The main objective of designing such flexible electronics is to offer the ideal devices for each application, regardless of the market segment.

2Solve's competencies in automation, electrical, electronic, and telecommunications engineering, combined with the flexibility of the 2Sense product allows the implementation of automation systems perfectly adjusted in quality, robustness, and cost.

Av. Fernando Ferrari, 1080
Ed. América Centro Empresarial
Torre Central, sala 403
Mata da Praia, Vitória/ES
29066-380

2Solve
ENGENHARIA E TECNOLOGIA

2Sense

The power supply options enable the use of chargeable, non-rechargeable batteries, DC sources from 9 to 36vdc and photovoltaic cells, or solar panels directly connected to 2Sense, which would act as a battery charge controller.

The hibernation time settings for acquisition/power of sensors and communication modules provide high battery performance, and in the configuration with an integrated solar panel, this functionality allows the use of much smaller cells.

Depending on the sleep mode setting, 2Sense will consume only **60 microamps**.

Depending on the connected sensors, battery technologies, and sample time, it is possible to perform measurements and data transmission for up to 5 years at a very low cost.

The application of inputs, outputs, ports, and other resources presented in the table of technical specifications is not possible in its entirety, that is, it is possible to implement a combination of resources that is limited by the physical capabilities of the electronics..

The combination of 2Sense features can enable a multitude of architectures to meet the demands of sensing and control.

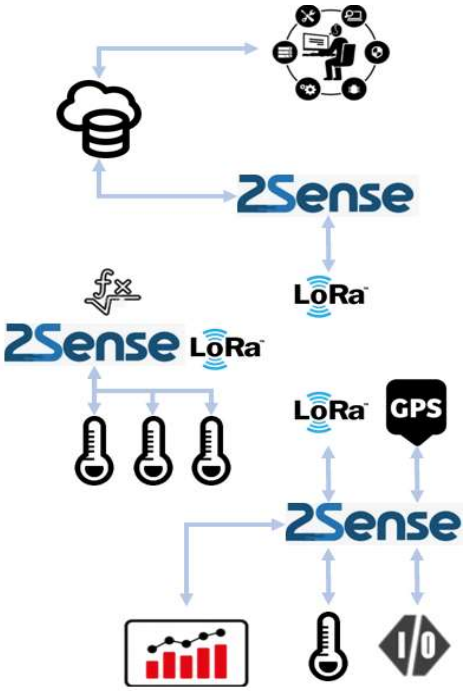

The combination of hardware resources and technical competence results in lean physical installations, with panels of low complexity of assembly and maintenance.

We want to know your demand so that together we can design the best solution.

In addition to offering hardware solutions for conventional automation applications, our business model seeks to partner with experts and demanders to develop specific solutions.

Av. Fernando Ferrari, 1080
Ed. América Centro Empresarial
Torre Central, sala 403
Mata da Praia, Vitória/ES
29066-380

2Solve
ENGENHARIA E TECNOLOGIA

Electrical connections:

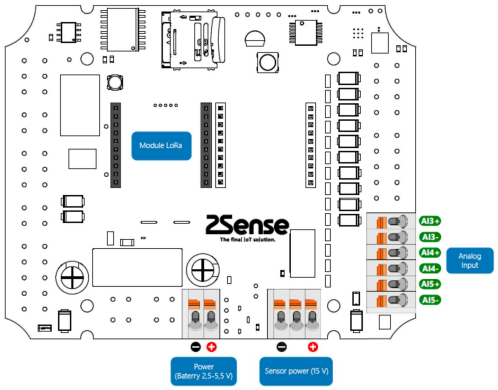

Optional aluminum housing:

Dimensions:

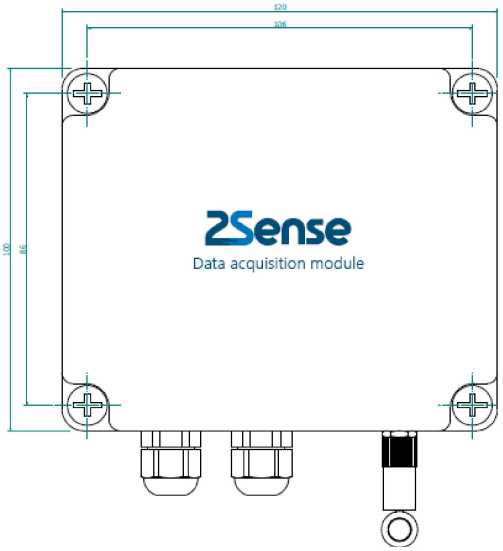

Av. Fernando Ferrari, 1080
Ed. América Centro Empresarial
Torre Central, sala 403
Mata da Praia, Vitória/ES
29066-380

2Solve
ENGENHARIA E TECNOLOGIA

Basic specifications

Conventional I/O options

√ 1 Digital input / pulse input
√ 1 Digital output
√ 2 Analog inputs 12bits (4-20mA or 0-10V)
√ 3 Analog inputs 24bits (4-20mA or 0-10V)
√ 1 input for temperature sensors (options PT100, PT1000 and Termopar)
√ 1 strain gauge input or load cell input
√ 15VDC output for sensors sensor supply

Integrated I/O (optional)

√ Accelerometer
√ Gyroscope
√ Magnetometer
√ GPS
√ Processor temperature
√ Battery charge

1 Shared digital Bus

√ I^2C
√ 1-Wire

Configuration (physical interface)

√ Local: USB 2.0
√ Remote: LoRa, Xbee, Sigfox, 2G, 3G, Ethernet/Modbus TCP

Serial communication

√ Modbus mster or slave
√ RS485 or RS232

Communication

√ Wireless:
√ LoRa
√ Xbee
√ Sigfox
√ 2G
√ 3G (developing)

Wired:
√ Ethernet/Modbus TCP (RJ45)

Display

√ I^2C Bus
√ IHM Modbus TCP

Datalogger function

√ SD card up to 32GB

Power options

√ 12/24 V Isolated
√ 12/24 V Not isolated
√ 2.5/5,5 Non-chargeable battery
√ 2.5/5,5 Chargeable battery/solar panel

Av. Fernando Ferrari, 1080
Ed. América Centro Empresarial
Torre Central, sala 403
Mata da Praia, Vitória/ES
29066-380

2Solve
ENGENHARIA E TECNOLOGIA

Resource configuration table			
Resources	**Type**	**Maximum quantity**	**Possible combinations**
Conventional I/O options	**Digital input / pulse input**	**1**	**NAT**
	Digital output	**1**	**NAT**
	Analogue inputs 24bits (4-20mA or 0-10V)	**3**	**C1**
	Input PT100, PT1000 and Termopar	**1**	**C1**
	Input strain gauge or load cell	**1**	**EP**
	Output 15 VDC for sensors sensor supply	**1**	**EP**
I/O integrated (optional)	Accelerometer	1	EP
	Gyroscope	1	EP
	Magnetometer	1	EP
	GPS	2	
	Processor temperature	1	NAT
	Battery charge/input DC	1	NAT
Datalogger Function	**SD card slot up to 32GB**	**1**	**NAT**
Display	I^2C Bus	1	OPT
	IHM Modbus TCP	1	OPT
	SPI Bus	1	OPT
1 Shared digital Bus	**I^2C**	**1**	**NAT**
	1-Wire	**1**	**NAT**
Serial communication	Modbus master or slave	1	C1
	RS232	1	C1
	RS485	1	C1
Additional communication technologies	**LoRa**	**2**	**Note 1**
	Xbee	**2**	
	Sigfox	**2**	
	2G	**2**	
	3G (developing)	**2**	
	Ethernet/Modbus TCP (RJ45)	**2**	

Observations	
Note 1:	**The 2 sense has two slots that can receive two communication technologies or a GS module, these being the same or different, working in redundancy or in isolation**
C1:	**Choose one of the resource**
EP:	**Optional features always possible to supply regardless of the desired configuration**
NAT:	**Native device feature**
OP:	**Optional accessory**

Av. Fernando Ferrari, 1080
Ed. América Centro Empresarial
Torre Central, sala 403
Mata da Praia, Vitória/ES
29066-380

2Solve
ENGENHARIA E TECNOLOGIA

Related products:

2Stools OV
OverView

2Stools IC
Industrial Computer

Visite: www.2solve.com

Watch our videos on the 2Solve YouTube channel.

Av. Fernando Ferrari, 1080
Ed. América Centro Empresarial
Torre Central, sala 403
Mata da Praia, Vitória/ES
29066-380

2Solve
ENGENHARIA E TECNOLOGIA

2STools Industrial Computer (IC) is a hybrid automation solution that combines industrial computer and programmable logic controller functionality.

Using **2SToolsIC** it is possible to acquire data and images, enabling real-time monitoring and control of processes and equipment.

This device is part of a family of automation products designed for IoT / Industry 4.0 designed to make automation of industrial processes easier and cheaper. This makes the 2SToolsIC a universal solution independent of the market segment.

Because it is a hybrid of industrial computer and PLC, **2SToolsIC** can have configured logic, have specific software running dedicated routines, or ship complementary software and join together acquired data (IO) and software functionality from other developers. Logics can use physical inputs and outputs, variables and mapped parameters from another device, or virtual inputs and outputs resulting from logic. Such logic can be programmed through the **2SToolsIC Device Manager** interface, which uses the concept of "object-oriented programming". So just fill in text fields, lists of options and checkboxes. This concept of programming eliminates the need for knowledge about programming languages, just knowing the logic to be implemented.

Also is possible to program logic as a ladder concept or in blocks using the Node Red tool.

If 2SToolsIC is used as part of a "locked" system, simply load the specific code into memory. Thus it is possible to transform the device into part of a system dedicated to a specific function. This product was developed to guarantee flexibility for the most diverse applications.

Just as a PLC has "cards", **2SToolsIC** has a family of **Extension Boards**, thus giving numerous features. This provides easy adaptation to any plant or equipment, regardless of size.

The **2SToolsIC** has natively digital inputs and outputs, pulse input and RS485 RTU communication. **Extension Boards** can add functions such as RTD (temperature), active or passive analog inputs, analog outputs, additional digital inputs and outputs, or other I / O cards developed on demand.

A major product differential is the ability to integrate i^2C, one wire, SPI and UART digital sensors. Such a feature dramatically increases the power of 2SToolsIC, because by using such a concept, it is possible to integrate dozens of sensors into a single device. Much more than the number of sensors, the concept enables the simultaneous integration of sensors of diverse purposes, all in one bus.

Using digital sensors it is possible to integrate, for example, measurements of humidity, temperature, vibration, luminosity, sound, etc.

Av. Fernando Ferrari, 1080
Ed. América Centro Empresarial
Torre Central, sala 403
Mata da Praia, Vitória/ES
29066-380

C 2SToolsIC Commercial Folder

2Solve
ENGENHARIA E TECNOLOGIA

The Communication Board is primarily responsible for enabling device integration into master and slave networks and devices. The flexibility that **Communication Board** offers is another great advantage of **2SToolsIC**. The modular feature of the board allows you to add functions such as WiFi, Ethernet, GPRS, GPS, among other technologies and protocols, including **narrow band IoT** technologies such as LoRa, Sigfox or even XBee, which can easily create mesh networks, the cost with communication infrastructure.

2SToolsIC also has USB ports and Ethernet ports.

USB ports can be used for IO expansion, making it possible to connect inexpensive expansion modules. In addition, they can enable the connection of other automation devices, converters and peripherals such as keyboards and others dedicated to data entry.

As for Ethernet ports, in addition to enabling the integration of 2SToolsIC into networks of different natures, you can also integrate other devices in this way.

Thanks to the flexibility of application of resources, Ethernet ports can be Power over Ethernet (PoE), making it possible to power security cameras and broadcast radios, for example.

2SToolsIC can still operate as a Wi-Fi network access point. With this, you can access settings, control equipment, view process or diagnostic variables, and even create a local area network enabling mobile access for voice and video communication . In addition to the features for I / O integration, 2STools IC has an intuitive graphical interface, allowing visualization of variables, configurations, graphics and execution of local and remote commands through the device. The embedded graphical interface eliminates the need to install configuration software, thus avoiding incompatibility disorders. Developed in "Angular", the responsive interface adapts to the screen of any device.

Thanks to the HDMI port and the USB ports, simply connect peripherals so that the 2STools IC is used as a powerful desktop.

A technological complement to the 2SToolsIC family is the 2SToolsIC Remote IO module. Using this device, it is possible to expand the capacity of inputs, outputs and communication ports using RS485 / 232 modbus wired serial communication, or wireless transmission technologies, such as LoRa or ZigBee.

The application of the 2SToolsIC Remote IO module, combined with, for example, ZigBee technology reduces the costs of integration between remote points, applying point-to-point, multipoint or mesh concepts.

The main purpose of designing such flexible electronics is to provide the ideal devices for each application regardless of market segment.

2Solve's competencies in automation, electrical, electronics and telecommunications engineering, coupled with the flexibilities of 2SToolsIC products, provide the implementation of automation systems perfectly adjusted for quality, robustness and cost.

Aesthetically, the combination of hardware capabilities and technical expertise results in lean physical installations with low complexity assembly and maintenance panels.

We want to know your demand so that together we can design the best solution.

In addition to offering hardware solutions for conventional automation applications, our business model seeks to partner with specialists and demanders to develop specific solutions.

Av. Fernando Ferrari, 1080
Ed. América Centro Empresarial
Torre Central, sala 403
Mata da Praia, Vitória/ES
29066-380

2Solve
ENGENHARIA E TECNOLOGIA

Basic technical specifications from 2SToolsIC Industrial Computer:

- BCM2837 Processor (1Gbyte LPDDR2 RAM)
- Operational System Linux (option with Windows)
- Serial port communication RS232/RS485
- HDMI port
- Power LED status
- SD Card slot up to 32GB
- Real-time Clock
- 3 digital inputs 24Vdc (Isolated - 1000 Vac)
- 2 digital relay outputs (300mA with 125Vac, 1A with 30 VDC / Isolated - 1000 Vac)
- 1 active pulse input 12Vdc 1kHz (Isolated - 1000 Vac)
- 1 USB 2.0 port universal
- 1 USB 2.0 port for I/O expansion
- 1 Ethernet Port compatible 10/100Mbps (option for PoE 12Vdc 10W Isolated 1500V)
- 1 Ethernet Port compatible 10/100Mbps (option PoE 24Vdc 8W Isolated 1500V)
- 1 slot for I/O "Extension board".

- Wireless communication:
  - Wi-Fi 802.11b/g/n module
  - ZigBee wireless module Digi XBee-PRO® 915MHz
  - LoRaWAN ou LoRa Mesh wireless module 915MHz RadioEnge
  - Sigfox wireless module

- Programming:
  - 2STools IC Device Manager
  - Ladder with CodeSys or Open PLC
  - Node RED blocks
  - Low-Level programming with Python

IMPORTANT:

We can design specifics Extension boards on request.

Technologies and their differentials

Av. Fernando Ferrari, 1080
Ed. América Centro Empresarial
Torre Central, sala 403
Mata da Praia, Vitória/ES
29066-380

2Solve
ENGENHARIA E TECNOLOGIA

Local and remote configuration and monitoring interface

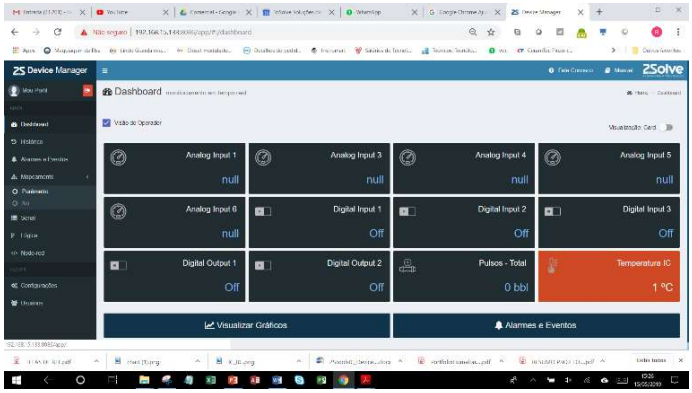

Intutitive embedded dashboard

- ✓ Web access with encrypted password
- ✓ Configurable Access Profile
- ✓ Quick view of variable status
- ✓ Responsive interface
- ✓ Compatible with PC, smartphone, tablets, etc.

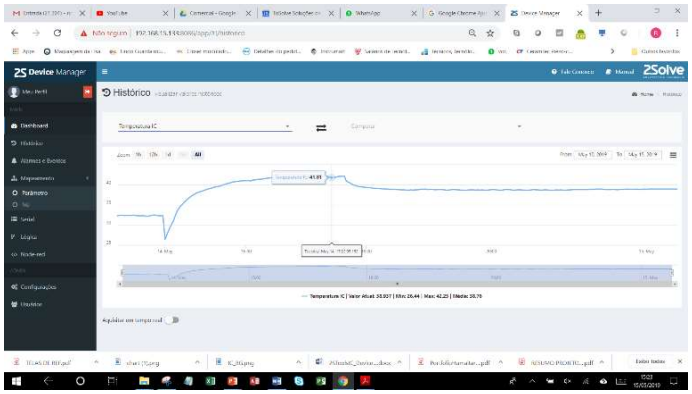

Trend Charts

- ✓ Realtime and historical variable visualization
- ✓ Period selection in bars and calendar
- ✓ Cursor with variable labels
- ✓ Export graphics image in pdf, svg, png and jpeg formats
- ✓ Comparison between variables

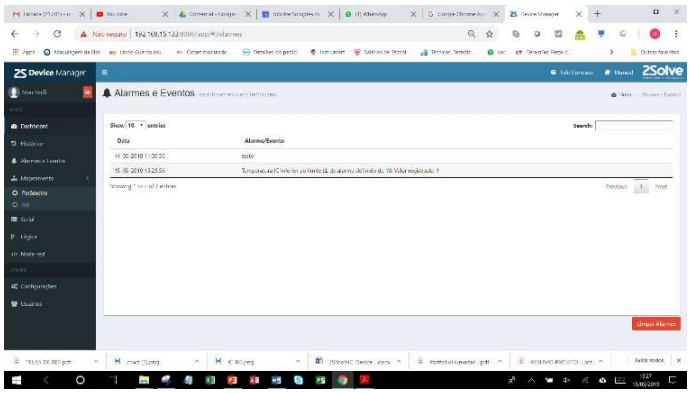

Alarm List

- ✓ Date
- ✓ Time
- ✓ Variable
- ✓ Alarm Description
- ✓ Corrective action suggestion

Av. Fernando Ferrari, 1080
Ed. América Centro Empresarial
Torre Central, sala 403
Mata da Praia, Vitória/ES
29066-380

2Solve
ENGENHARIA E TECNOLOGIA

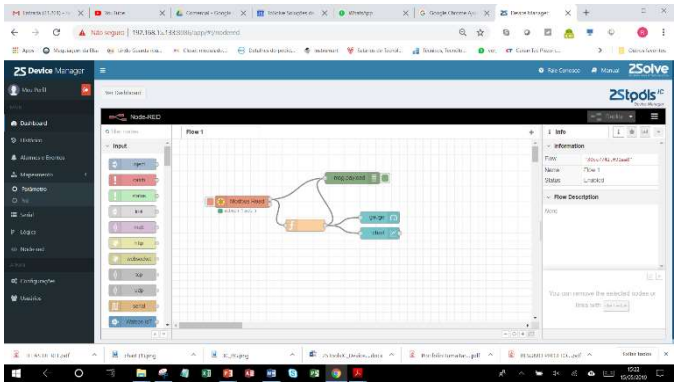

Programming Tools

- ✓ Embedded interface with web browser access
- ✓ Device Manager proprietary interface configuration
- ✓ Block programming with Node-RED
- ✓ Ladder Programming with Codesys and Open PLC

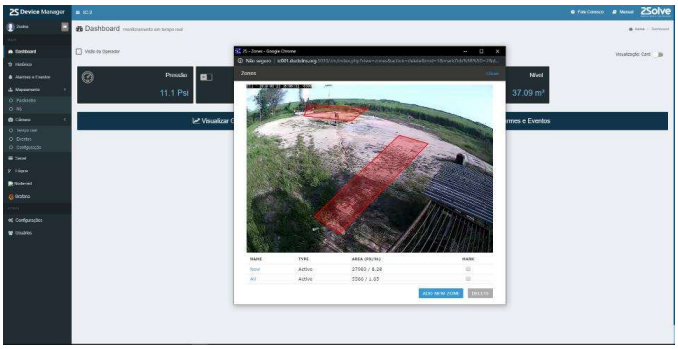

Monitoring and logic by image

- ✓ Motion Detection
- ✓ Alarms integrated with automation logic

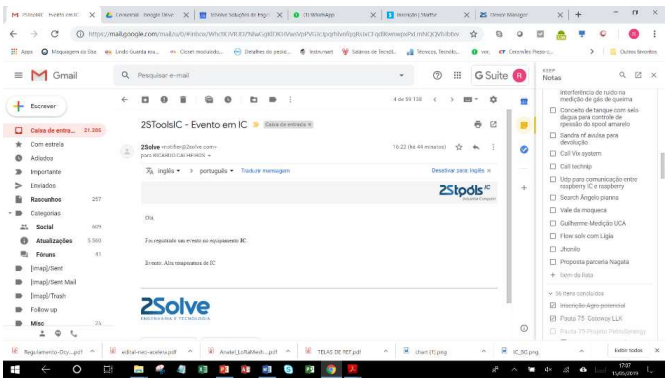

E-mailalarms

- ✓ Profile driven alarms
- ✓ Failure detected and suggested action

Av. Fernando Ferrari, 1080
Ed. América Centro Empresarial
Torre Central, sala 403
Mata da Praia, Vitória/ES
29066-380

2Solve
ENGENHARIA E TECNOLOGIA

CPU
√ BCM2837 processor (1Gbyte LPDDR2 RAM)
√ Linux operating system (Windows option)
√ HDMI port
√ One slot for installing an I / O expansion board "Extension board"

Configuration/programming options
√ 2Stools IC Device Manager
√ Ladder (Codesys or Open PLC)
√ Node RED
√ C
√ Python

Integrated I/O
√ Three 24Vdc digital inputs (Isolated - 1000 Vac)
√ Two digital relay outputs (300mA with 125Vac, 1A with 30VDC / Isolated - 1000Vac)
√ One active pulse input 12Vdc 5 kHz (Isolated - 1000 Vac)
√ GPS (optional)
√ Processor temperature

Protocols
√ Modbus TCP
√ RS232
√ RS485
√ Modbus RTU
√ Ethernet
√ MQTT

Native communication
√ RS232/RS485 serial communication port
√ Modbus master or slave
√ One universal USB 2.0 port
√ One USB 2.0 port for I/O expansion
√ One compatible 10/100Mbps Ethernet port (option for Poe 12Vdc 10W Isolated 1500V)
√ One 10/100Mbps compatible Ethernet port (Poe option 24Vdc 8W isolated 1500V)

Configuration (physical interface)
√ Local: USB 2.0
√ Remote: LoRa, Xbee, Sigfox, 2G, 3G, Ethernet/Modbus TCP

Power options
√ 12 isolated vdc
√ 24 isolated vdc

Datalogger function
√ SD card up to 32GB

Display (optional)
√ I²C bus
√ IHM Modbus TCP

Optional communication (1 solot): Wireless:
√ LoRa
√ Xbee
√ Sigfox
√ 2G
√ 3G (developing)

Wired:
√ Ethernet/Modbus TCP (RJ45)

Digital bus option for sensors
√ I²C
√ 1-Wire

Av. Fernando Ferrari, 1080
Ed. América Centro Empresarial
Torre Central, sala 403
Mata da Praia, Vitória/ES
29066-380

2Solve
ENGENHARIA E TECNOLOGIA

Dimensions

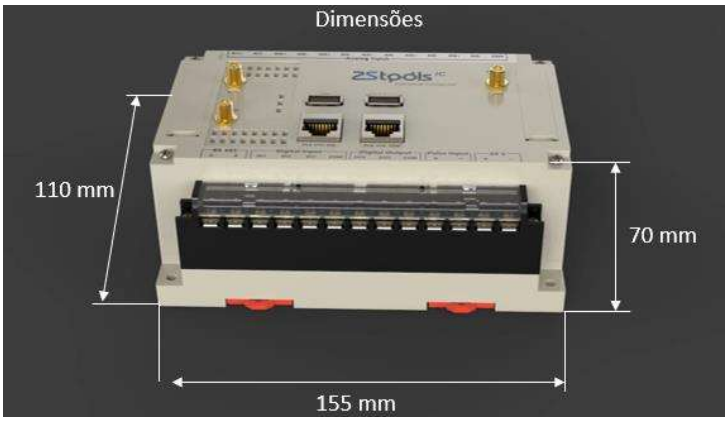

Related products:

2Stools IC
Remote I/O

2Stools OV
OverView

2Sense

Visit: www.2solve.com

Av. Fernando Ferrari, 1080
Ed. América Centro Empresarial
Torre Central, sala 403
Mata da Praia, Vitória/ES
29066-380

2Solve
ENGENHARIA E TECNOLOGIA

Watch our videos on 2Solve

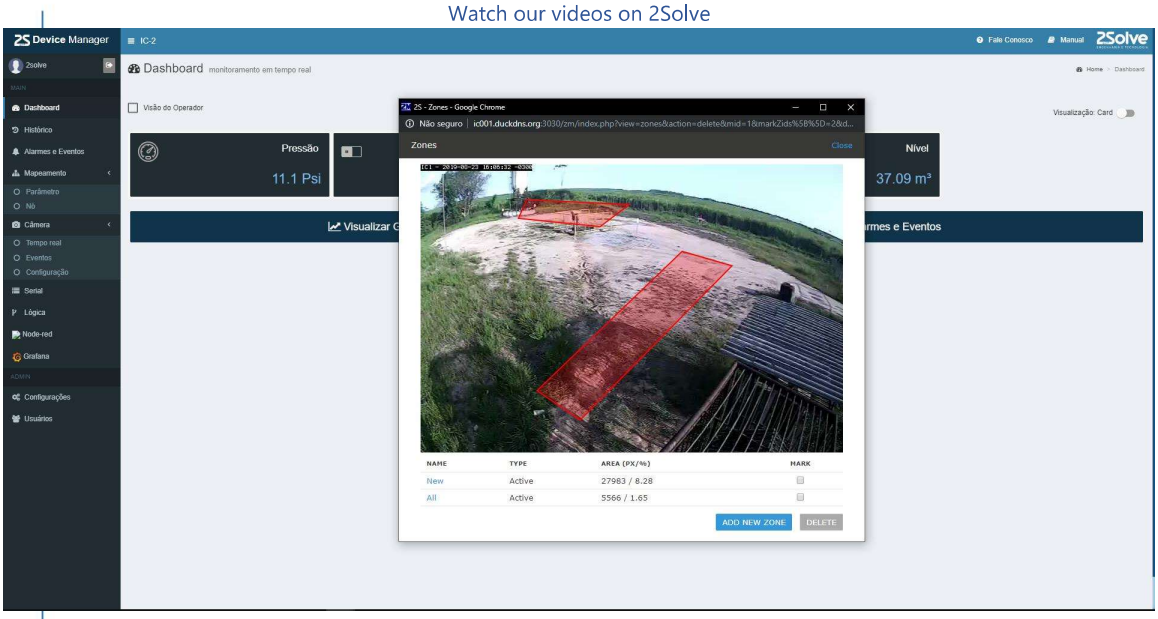

on YouTube

Av. Fernando Ferrari, 1080
Ed. América Centro Empresarial
Torre Central, sala 403
Mata da Praia, Vitória/ES
29066-380

D Configuration of the LoRaWan Gateway used in the Experiments

/opt/ttn-gateway/bin/local_conf.json

```
{
  "SX1301_conf": {
    "lorawan_public": true,
        "clksrc": 1,
        "clksrc_desc": "radio_1 provides clock to concentrator for
         most devices except MultiTech. For MultiTech set to 0.",
        "antenna_gain": 0,
        "antenna_gain_desc": "antenna gain, in dBi",
        "radio_0": {
                "enable": true,
                "type": "SX1257",
                "freq": 917200000,
                "rssi_offset": -166.0,
                "tx_enable": true,
                "tx_freq_min": 915000000,
                "tx_freq_max": 928000000
        },
        "radio_1": {
                "enable": true,
                "type": "SX1257",
                "freq": 917900000,
                "rssi_offset": -166.0,
                "tx_enable": false
        },
        "chan_multiSF_0": {
                "desc": "Lora MAC, 125kHz, all SF, 916.8 MHz",
                "enable": true,
                "radio": 0,
                "if": -400000
        },
```

```
"chan_multiSF_1": {
        "desc": "Lora MAC, 125kHz, all SF, 917.0 MHz",
        "enable": true,
        "radio": 0,
        "if": -200000
},
"chan_multiSF_2": {
        "desc": "Lora MAC, 125kHz, all SF, 917.2 MHz",
        "enable": true,
        "radio": 0,
        "if": 0
},
"chan_multiSF_3": {
        "desc": "Lora MAC, 125kHz, all SF, 917.4 MHz",
        "enable": true,
        "radio": 0,
        "if": 200000
},
"chan_multiSF_4": {
        "desc": "Lora MAC, 125kHz, all SF, 917.6 MHz",
        "enable": true,
        "radio": 1,
        "if": -300000
},
"chan_multiSF_5": {
        "desc": "Lora MAC, 125kHz, all SF, 917.8 MHz",
        "enable": true,
        "radio": 1,
        "if": -100000
},
"chan_multiSF_6": {
        "desc": "Lora MAC, 125kHz, all SF, 918.0 MHz",
        "enable": true,
        "radio": 1,
        "if": 100000
},
"chan_multiSF_7": {
        "desc": "Lora MAC, 125kHz, all SF, 918.2 MHz",
        "enable": true,
```

```
        "radio": 1,
        "if": 300000
    },
    "chan_Lora_std": {
        "desc": "Lora MAC, 500kHz, SF8, 917.5 MHz",
        "enable": true,
        "radio": 0,
        "if": 300000,
        "bandwidth": 500000,
        "spread_factor": 8
    },
    "chan_FSK": {
        "desc": "disabled",
        "enable": false
    },
    "tx_lut_0": {
        "desc": "TX gain table, index 0",
        "pa_gain": 0,
        "mix_gain": 8,
        "rf_power": -6,
        "dig_gain": 0
    },
    "tx_lut_1": {
        "desc": "TX gain table, index 1",
        "pa_gain": 0,
        "mix_gain": 10,
        "rf_power": -3,
        "dig_gain": 0
    },
    "tx_lut_2": {
        "desc": "TX gain table, index 2",
        "pa_gain": 0,
        "mix_gain": 12,
        "rf_power": 0,
        "dig_gain": 0
    },
    "tx_lut_3": {
        "desc": "TX gain table, index 3",
        "pa_gain": 1,
```

```
            "mix_gain": 8,
            "rf_power": 3,
            "dig_gain": 0
    },
    "tx_lut_4": {
            "desc": "TX gain table, index 4",
            "pa_gain": 1,
            "mix_gain": 10,
            "rf_power": 6,
            "dig_gain": 0
    },
    "tx_lut_5": {
            "desc": "TX gain table, index 5",
            "pa_gain": 1,
            "mix_gain": 12,
            "rf_power": 10,
            "dig_gain": 0
    },
    "tx_lut_6": {
            "desc": "TX gain table, index 6",
            "pa_gain": 1,
            "mix_gain": 13,
            "rf_power": 11,
            "dig_gain": 0
    },
    "tx_lut_7": {
            "desc": "TX gain table, index 7",
            "pa_gain": 2,
            "mix_gain": 9,
            "rf_power": 12,
            "dig_gain": 0
    },
    "tx_lut_8": {
            "desc": "TX gain table, index 8",
            "pa_gain": 1,
            "mix_gain": 15,
            "rf_power": 13,
            "dig_gain": 0
    },
```

```
"tx_lut_9": {
        "desc": "TX gain table, index 9",
        "pa_gain": 2,
        "mix_gain": 10,
        "rf_power": 14,
        "dig_gain": 0
},
"tx_lut_10": {
        "desc": "TX gain table, index 10",
        "pa_gain": 2,
        "mix_gain": 11,
        "rf_power": 16,
        "dig_gain": 0
},
"tx_lut_11": {
        "desc": "TX gain table, index 11",
        "pa_gain": 3,
        "mix_gain": 9,
        "rf_power": 20,
        "dig_gain": 0
},
"tx_lut_12": {
        "desc": "TX gain table, index 12",
        "pa_gain": 3,
        "mix_gain": 10,
        "rf_power": 23,
        "dig_gain": 0
},
"tx_lut_13": {
        "desc": "TX gain table, index 13",
        "pa_gain": 3,
        "mix_gain": 11,
        "rf_power": 25,
        "dig_gain": 0
},
"tx_lut_14": {
        "desc": "TX gain table, index 14",
        "pa_gain": 3,
        "mix_gain": 12,
```

```
                "rf_power": 26,
                "dig_gain": 0
        },
        "tx_lut_15": {
        "desc": "TX gain table, index 15",
        "pa_gain": 3,
        "mix_gain": 14,
        "rf_power": 27,
        "dig_gain": 0
        }
        },
  "gateway_conf": {
        "gateway_ID": "B827EBFFFEC90112",
        "servers": [ { "server_address": "router.us.thethings.network",
        "serv_port_up": 1700, "serv_port_down": 1700,
        "serv_enabled": true } ],
        "ref_latitude": 0,
        "ref_longitude": 0,
        "ref_altitude": 0,
        "contact_email": "",
        "description": "GW_RAK831_VV"
  }
}
```